A second-order well-balanced Lagrange-projection scheme for Shallow Water Exner equations in 1D and 2D

Christophe Chalons, Alessia del Grosso

A second-order well-balanced Lagrange-projection scheme for Shallow Water Exner equations in 1D and 2D

C. Chalons*and A. Del Grosso†

June 7, 2021

Abstract. The present work is devoted to the numerical approximation of the Shallow water Exner system in both one and two dimensions, where the Exner equation expresses the evolution in time of the bed sediment. In particular the Grass formula is taken into account to model the solid transport discharge contributions. The numerical scheme is based on the Lagrange-projection formalism which consists in splitting the mathematical model into the acoustic and transport system. In particular, the Exner equation is taken into account only at the transport level; both a decoupled and weakly coupled formulation are proposed. The method is designed in such a way to satisfy the well-balanced property as well. Details to reach the second-order of accuracy are given; numerical results are shown to validate the numerical schemes.

1 Introduction and governing equations

This work deals with the design and implementation of a second-order well-balanced Lagrange-projection scheme applied to the 1D and 2D shallow water system with bed sediment not-constant in time. Lagrange-projection approach consists in splitting the acoustic and transport waves of the model, leading to the possibility of approximating the two resulting systems with different approaches. This reveals itself to be useful for instance in subsonic regimes, where the acoustic waves are the reason of the restrictive CFL condition one has to employ in order to have a stable numerical scheme. Indeed, the Lagrange-projection decomposition makes possible to implicitly approximate only the acoustic system and, thus, to circumnavigate the problem of restrictive time-steps.

Nowadays, the Lagrange-projection approach have been studied in order to satisfy different properties and as applied to several models. Giving few examples, we refer for instance to the work [21], where all-regime first-order explicit and semi-implicit Lagrange-projection schemes have been applied to the gas dynamics model in several dimensions, or to [20], where the scheme was extended to the 2D two-phase flows model. Another possible reference is [8] with the numerical approximation of low Mach number flows of the barotropic Euler equations where the asymptotic-preserving property is satisfied as well. On the other hand, when it comes to the modeling of the shallow water system in the Lagrange-projection formalism, we can refer to [22] for an implicit well-balanced first-order scheme, to [15] for a fully well-balanced first-order explicit method, and finally to [40] for high-order fully well-balanced schemes. Last but not least, and without being exhaustive, we refer for instance to [27, 37, 35, 13, 43] for other interesting studies in this framework.

While details for the Lagrange-projection splitting are given in the following section, let us present now the mathematical model we are interested in. It is composed of two different ones, the hydrodynamic and the morphodynamic model. The former is simply given by the well-known shallow water system, which is derived from the Navier-Stokes system under the hypothesis that the vertical scale is much smaller than the horizontal dimension. As such, it is composed of the continuity and momentum equations, which are expressed as in the following

$$\begin{cases} \partial_t h + \partial_x(hu) = 0 \\ \partial_t(hu) + \partial_x(hu^2 + \frac{gh^2}{2}) = -gh\partial_x z \end{cases} \tag{1.1}$$

*Laboratoire de Mathématiques de Versailles, UMR 8100, Université de Versailles Saint-Quentin-en-Yvelines, UFR des Sciences, bâtiment Fermat, 45 avenue des Etats-Unis, 78035 Versailles cedex, France. E-mail: christophe.chalons@uvsq.fr

†Laboratoire de Mathématiques de Versailles, UMR 8100, Université de Versailles Saint-Quentin-en-Yvelines, UFR des Sciences, bâtiment Fermat, 45 avenue des Etats-Unis, 78035 Versailles cedex, France. E-mail: alessia.del-grosso2@uvsq.fr

where $h(x,t) > 0$ is the water depth, $u(x,t)$ the averaged velocity and $z(x,t)$ the bed level. In particular, $H = h + z$ is the free surface elevation. Finally, g is the gravitational acceleration, $t > 0$ represents the time and x the axial coordinate. Let us briefly recall that this system is strictly hyperbolic with real eigenvalues given by $u \pm c$ with the sound speed $c = \sqrt{gh}$.

Then, we aim to simulate the interaction between the sediments and the flow, thus we consider the topography z not constant in time and we make use of the so-called Exner equation, which reads

$$\partial_t z + \zeta \partial_x q_b = 0. \tag{1.2}$$

Here $q_b = q_b(h,u)$ is the solid transport discharge, $\zeta = \frac{1}{1-\rho_0}$ and ρ_0 is the porosity of the sediment layer. The coupling of (1.1) and (1.2) leads to the final system,

$$\begin{cases} \partial_t h + \partial_x (hu) = 0 \\ \partial_t (hu) + \partial_x (hu^2 + \frac{gh^2}{2}) + gh\partial_x z = 0 \\ \partial_t z + \zeta \partial_x q_b = 0, \end{cases} \tag{1.3}$$

which in compact form reads

$$\partial_t \mathbf{Q} + \partial_x \mathbf{F}(\mathbf{Q}) + \mathbf{A}(\mathbf{Q})\partial_x \mathbf{Q} = \mathbf{O}$$

where

$$\mathbf{Q} = \begin{pmatrix} h \\ hu \\ z \end{pmatrix}, \quad \mathbf{F}(\mathbf{Q}) = \begin{pmatrix} hu \\ hu^2 + p \\ \zeta q_b \end{pmatrix}, \quad \mathbf{A}(\mathbf{Q}) = \begin{pmatrix} 0 & 0 & 0 \\ 0 & 0 & gh \\ 0 & 0 & 0 \end{pmatrix}$$

with the pressure term $p = \frac{gh^2}{2}$. For details about shallow-water equations with and without not-constant in time bed sediment, we refer for instance to [2, 9, 10, 7] and [47, 3, 12, 15, 41].

It is known that there exist different formulations to express the solid transport discharge q_b, depending on the characteristics of the sediment and the flow, for instance the Froude number, the slope of the bottom or the grain size. One of the easiest and most frequently used formulation is the well-known Grass model, which expresses the instantaneous sediment transport as a power law of the averaged velocity u, namely

$$q_b = A_g u |u|^{m_g - 1}, \quad 1 \leq m_g \leq 4, \tag{1.4}$$

refer to [42, 5]. This deterministic Grass formulation is suitable to model non-cohesive granular sediment. Here $A_g \in [0,1]$ is a dimensional calibration constant which is usually measured experimentally and expresses the kind of interaction between the fluid and the sediment, whose strength increases as A_g approaches to 1. In particular, the value of the constant A_g is related to factors as the grain size and the kinematic viscosity. Finally, we set $m_g = 3$.

In this work we will take into account only the Grass model, but for details about other possible formulations for the solid transport discharge, refer to [42]. It is important to stress that, depending on the formulation used for q_b, system (1.3) may be hyperbolic or not. In particular, in [10] it has been confirmed that considering the Grass formula leads to a strictly hyperbolic system with all real eigenvalues. Indeed, defining the quantities

$$a_1 = -2u, \quad a_2 = u^2 - c^2(1 + \zeta \partial_{hu} q_b) \quad \text{and} \quad a_3 = -\zeta c^2 \partial_h q_b,$$

one can easily see that the eigenvalues are given by the solution of the following equation

$$\lambda^3 + a_1 \lambda^2 + a_2 \lambda + a_3 = 0.$$

Hence, the three eigenvalues read

$$\lambda_k = 2\sqrt{-p}\cos(\frac{\theta + 2k\pi}{3}) - \frac{a_1}{3} \quad \text{with} \quad k = 0, 1, 2. \tag{1.5}$$

where

$$p = \frac{3a_2 - a_1^2}{9}, \quad r = \frac{9a_1 a_2 - 27a_3 + 2a_1^3}{54} \quad \text{and} \quad \theta = \arccos(\frac{r}{\sqrt{-p^3}}).$$

We remark that, in order to have real eigenvalues, we need $p^3 + r^2 \leq 0$, which can be proved in the case of the Grass model.

As mentioned at the very beginning of this work, we are also looking for a well-balanced numerical scheme, namely able to preserve the smooth stationary solutions of the system, that is to say the steady states which satisfy the ordinary differential equations

$$\partial_x(hu) = 0, \quad \partial_x(hu^2 + \frac{gh^2}{2}) + gh\partial_x z = 0 \quad \text{and} \quad \partial_x q_b = 0,$$

and obey to

$$q = hu = \text{constant} = q_0, \quad \frac{q_0^2}{2h^2} + g(h+z) = \text{constant} \quad \text{and} \quad q_b = \text{constant}.$$

Note that if we use the Grass formula for q_b, then the only non trivial stationary solutions are given by

$$u = 0 \quad \text{and} \quad h + z = \text{constant}, \tag{1.6}$$

which is called "lake at rest" equilibrium. For well-balanced schemes for the shallow-water equations, see for instance to [3, 12, 38, 39], while for well-balanced methods in the Lagrange-projection formalism we refer to [22, 15, 40]. As far as the evolution in time of the bed sediment is considered as well, for general well-balanced schemes we refer for instance to [5, 36].

Outline of the paper. For the sake of clarity, let us briefly give the paper structure. In the next section 2, the Lagrange-projection splitting is presented considering both Eulerian and Lagrangian variables. A brief summary of the approximate Riemann solver for the acoustic system is outlined as well. In section 3, both first and second-order numerical schemes are described, distinguishing between acoustic and transport step. Then, the two-dimensional extension of the mathematical model and numerical method is illustrated in section 4. Finally, section 5 is exploited to present the numerical results and validate our numerical schemes. Concluding, final remarks are drawn in section 6.

2 Operator splitting and Lagrangian coordinates

In this section we briefly explain the decomposition which entails the splitting of system (1.3) into two different ones, the so-called acoustic and transport systems. The former takes into account the acoustic effects of the model and the source term related to the topography, while the latter the transport phenomena. We will see further on that this splitting can be interpreted as a Lagrange-projection one, as we first formulate the shallow-water system in Lagrangian coordinates (acoustic step) and then we project the solution into Eulerian coordinates (transport step). For more the details about this decomposition, the reader can refer to [15, 22, 40].

Considering first only the shallow water system, it can be reformulated as

$$\begin{cases} \partial_t h + h\partial_x u + u\partial_x h = 0 \\ \partial_t(hu) + hu\partial_x u + u\partial_x(hu) + \partial_x(\frac{gh^2}{2}) = -gh\partial_x z, \end{cases}$$

where we used the chain rule for space derivatives. Therefore, the acoustic and transport system are respectively given by

$$\begin{cases} \partial_t h + h\partial_x u = 0 \\ \partial_t(hu) + hu\partial_x u + \partial_x(\frac{gh^2}{2}) = -gh\partial_x z, \end{cases} \tag{2.1}$$

and

$$\partial_t X + u\partial_x X = 0 \tag{2.2}$$

with $X = h$ and $X = hu$. We also observe that the acoustic system (2.1) can be expressed as

$$\begin{cases} \partial_t \tau - \partial_m u = 0 \\ \partial_t u + \partial_m p = -\frac{g}{\tau}\partial_m z \end{cases} \tag{2.3}$$

where we have introduced the unknown $\tau = \frac{1}{h}$ and the mass variable m such that $\frac{1}{h}\partial_x = \partial_m$, see [15, 23, 20, 21, 22]. Moreover, it is easy to find that the eigenvalues of system (2.3) are $\pm h\sqrt{gh} = \pm hc$.

About the Exner equation. Let us now consider the Exner equation as well, for which one could imagine at least three possibilities for numerical treatment. The first one would account for it at the acoustic level, the second one directly inside the transport step, and the third one by splitting it inside both steps. However, the issue of coupling the Exner equation and the shallow water system has been vastly studied in the literature. In particular, it is known that a fully decoupled scheme can lead to a numerical method which produces spurious oscillations inside the numerical solutions; this issue has been clearly presented in [26]. However, it is not even necessary to consider a fully coupled scheme in order to avoid this problem; indeed a weakly coupling of the equations at the numerical level can lead to satisfying results, see for instance [5]. In this work we mainly focus on weakly coupled numerical approach. Moreover, in the following we completely take into account the Exner equation in the projection step.

Finally, in this first part of this work, the acoustic and transport systems respectively read

$$\begin{cases} \partial_t \tau - \partial_m u = 0 \\ \partial_t u + \partial_m p = -\frac{g}{\tau}\partial_m z \\ \partial_t z = 0 \end{cases} \tag{2.4}$$

and

$$\begin{cases} \partial_t h + u\partial_x h = 0 \\ \partial_t (hu) + u\partial_x (hu) = 0 \\ \partial_t z + \zeta \partial_x q_b = 0. \end{cases} \tag{2.5}$$

Hence, the numerical strategy will be composed of two steps:

1. Take into account the acoustic effects of the model by solving system (2.4);
2. Consider and solve the transport system (2.5);

System (1.1) in Lagrangian coordinates. In order to interpret the strategy as a Lagrange-Projection one, we first define the fluid particle ξ and the characteristic curves

$$\begin{cases} \frac{\partial x}{\partial t}(\xi, t) = u(x(\xi, t), t) \\ x(\xi, 0) = \xi \end{cases} \tag{2.6}$$

which define the trajectory : $t \to x(\xi, t)$, of ξ as the time goes on. Therefore, any function : $(x, t) \to \varphi(x, t)$ in Eulerian coordinates can be written in Lagrangian coordinates,

$$\bar{\varphi}(\xi, t) = \varphi(x(\xi, t), t).$$

Let us now introduce the volume ratio

$$L(\xi, t) = \frac{\partial x}{\partial \xi}(\xi, t) \tag{2.7}$$

such that

$$\begin{cases} \frac{\partial L}{\partial t}(\xi, t) = \partial_\xi u(x(\xi, t), t) \\ L(\xi, 0) = 1. \end{cases} \tag{2.8}$$

Consequently, we note that

$$\partial_t L(\xi, t) = \partial_\xi u(x(\xi, t), t) = \partial_\xi \bar{u}(\xi, t),$$

and thus

$$\partial_\xi \bar{\varphi}(\xi, t) = L(\xi, t)\partial_x \varphi(x, t) \quad \text{and} \quad \partial_t \bar{\varphi}(\xi, t) = \partial_t \varphi(x, t) + u(x, t)\partial_x \varphi(x, t).$$

We have now all the ingredients to write (1.1) in Lagrangian coordinates. More precisely, observing that smooth solutions of (1.1) satisfy

$$\begin{cases} L(\partial_t h + u\partial_x h + h\partial_x u) = 0 \\ L(\partial_t (hu) + u\partial_x (hu) + hu\partial_x u + \partial_x p + gh\partial_x z) = 0 \end{cases}$$

and

$$\begin{cases} L\partial_t \bar{h} + \bar{h}\partial_t L = 0 \\ L\partial_t \overline{hu} + \overline{hu}\partial_t L + \partial_\xi \bar{p} + g\bar{h}\partial_\xi \bar{z} = 0 \end{cases}$$

we get

$$\begin{cases} \partial_t (L\bar{h}) = 0 \\ \partial_t (L\overline{hu}) + \partial_\xi \bar{p} = -g\bar{h}\partial_\xi \bar{z}. \end{cases} \tag{2.9}$$

Notice that in the following sections, we shall omit the bar over the Lagrangian functions when there can be no confusion. This new formulation of system (1.1) exploiting the Lagrangian coordinates makes the above numerical strategy based on an acoustic-transport splitting strictly equivalent to a Lagrangian-projection splitting, that can be summarized as in the following,

1. Solve the system (2.9) in Lagrangian coordinates;
2. Project the solution in Eulerian coordinates solving the transport system (2.5).

To conclude this section, we derive from (2.9) an evolution equation for Lu that will be useful in the next sections. Removing the bars and using the discharge equation on Lu, we have in particular

$$h\partial_t (Lu) + Lu\partial_t h + \partial_\xi p + gh\partial_\xi z = 0$$

and, since $0 = \partial_t (Lh) = h\partial_t L + L\partial_t h = h\partial_\xi u + L\partial_t h$, we get

$$h\partial_t (Lu) - hu\partial_\xi u + \partial_\xi p + gh\partial_\xi z = 0$$

and finally

$$\partial_t (Lu) - \partial_\xi \frac{u^2}{2} = -g\partial_\xi (h + z). \tag{2.10}$$

Note that the source term now involves the quantity $h + z$ which is constant for stationary solutions.

2.1 A well-balanced approximate Riemann solver for the acoustic system

In this section we briefly recall the definition of a well-balanced approximate Riemann solver proposed in [22] for the acoustic system (2.4) and that will be useful in the following. It is based on the Gallice theory [28, 29] which is an extension to balance laws of the Harten, Lax and van Leer formalism [32] for conservation laws. For more details about this Riemann solver, the reader can refer to [22]. Then, suppose that we want to solve (2.4) with the following Riemann initial data

$$\mathbf{U}(m, t = 0) = \begin{cases} \mathbf{U}_L & \text{if} \quad m < 0 \\ \mathbf{U}_R & \text{if} \quad m \geq 0 \end{cases}$$

where we have set

$$\mathbf{U}_L = \begin{pmatrix} \tau_L \\ u_L \\ z_L \end{pmatrix} \quad \text{and} \quad \mathbf{U}_R = \begin{pmatrix} \tau_R \\ u_R \\ z_R \end{pmatrix}.$$

The proposed approximate solution has the following form

$$\hat{\mathbf{U}}(\frac{m}{t}; \mathbf{U}_L, \mathbf{U}_R) = \begin{cases} \mathbf{U}_L & \text{if} \quad \frac{m}{t} < -a \\ \mathbf{U}_L^* & \text{if} \quad -a < \frac{m}{t} < 0 \\ \mathbf{U}_R^* & \text{if} \quad 0 < \frac{m}{t} < a \\ \mathbf{U}_R & \text{if} \quad \frac{m}{t} > a \end{cases}$$

where a is a constant and where the intermediate states

$$\mathbf{U}_L^* = \begin{pmatrix} \tau_L^* \\ u_L^* \\ z_L \end{pmatrix}, \quad \mathbf{U}_R^* = \begin{pmatrix} \tau_R^* \\ u_R^* \\ z_R \end{pmatrix} \tag{2.11}$$

are defined thanks to

$$\begin{cases} \tau_L^* = \tau_L + \dfrac{1}{a}(u_* - u_L) \\ \tau_R^* = \tau_R - \dfrac{1}{a}(u_* - u_R) \\ u_L^* = u_R^* = u^* \\ u^* = \dfrac{1}{2}(u_L + u_R) - \dfrac{1}{2a}(\Pi_R - \Pi_L) - \dfrac{\mathcal{M}}{2a} \\ \Pi^* = \dfrac{1}{2}(\Pi_L + \Pi_R) - \dfrac{a}{2}(u_R - u_L) \end{cases}$$

with

$$\mathcal{M} = \frac{g}{2}(\frac{1}{\tau_L} + \frac{1}{\tau_R})(z_R - z_L).$$

Observe that Π is a new variable introduced to be able to define the approximate Riemann solver. In particular, Π can be interpreted as a linearization of the pressure term p and its initial data are well-prepared in the sense that $\Pi = p$.

Then, it is clear that $\mathcal{M} = 0$ if $z_L = z_R$ so that the classical form of an approximate Riemann solver for a system of conservation law is recovered, while $X_L^* = X_L$ and $X_R^* = X_R$ with $X = \tau, u$, when the "lake at rest" stationary conditions are satisfied, namely

$$u_L = u_R = 0, \quad h_L + z_L = h_R + z_R.$$

In that sense, the proposed approximate Riemann solver is said to be well-balanced. Note that this is true whatever the definition of the constant a is. In practice, we will choose $a = \max((hc)_L, (hc)_R)$ according the well-known subcharacteristic stability condition. For more details, we refer again to [22].

3 Numerical methods

Before getting into the heart of the matter, we give few details about the time and space discretizations we use in the following sections. Given a constant time step Δt, we define the intermediate times by $t^n = n\Delta t$ for $n \in \mathbb{N}$. Then, the mesh interfaces are $x_{j+1/2} = j\Delta x$ for $j \in \mathbb{Z}$, where Δx is the constant space step, while x_j is the center of the cell $[x_{j-1/2}, x_{j+1/2})$. Hence, given a variable φ, we denote φ_j^n its constant average approximation on each cell $[x_{j-1/2}, x_{j+1/2})$ at time t^n, namely

$$\varphi_j^n \approx \frac{1}{\Delta x} \int_{x_{j-1/2}}^{x_{j+1/2}} \varphi(x, t^n)\, dx,$$

with $n \in \mathbb{N}$ and $j \in \mathbb{Z}$. At last, note that, regarding the mass variable m, we use $\Delta m_j = h_j^n \Delta x$ for all j.

Given the sequence $\{\varphi_j^n\}_j$, we now look for its approximation at the next time level t^{n+1}, namely $\{\varphi_j^{n+1}\}_j$. At this stage, we are able to present the numerical schemes, starting with the first-order method and proceeding with the second-order one. For each of them, we will prove the well-balanced condition as well. Let us recall that the numerical schemes are divided into two different steps. First we have the acoustic step, in which we numerically solve system (2.4). Then, we exploit its solution as the initial condition for solving system (2.5). We can sum up this procedure in the following way,

1. Acoustic step: solve system (2.4) in order to update $\mathbf{Q}^n$ to $\mathbf{Q}^{n+1-}$;
2. Transport step: find $\mathbf{Q}^{n+1}$ from $\mathbf{Q}^{n+1-}$ by the approximation of the solution of system (2.5).

Note that in the first step, we implicitly use the change of variable $\mathbf{U} = \mathbf{U}(\mathbf{Q})$ to first define $\mathbf{U}^n$ from $\mathbf{Q}^n$ before solving (2.4), and then the change of variables $\mathbf{Q} = \mathbf{Q}(\mathbf{U})$ to define $\mathbf{Q}^{n+1-}$ from $\mathbf{U}^{n+1-}$.

3.1 First-order scheme

Here we give the details for the first-order scheme distinguishing between the acoustic and transport steps.

3.1.1 Acoustic step and Lagrangian reformulation

As far as the discretization of (2.4) is concerned, we suggest to use a classical Godunov-type method based on the well-balanced approximate Riemann solver proposed in section 2.1. As usual, it simply consists in averaging on each cell the juxtaposition of the approximate Riemann solutions set at each interface. Therefore, it follows after easy calculations that the numerical discretization of the acoustic relaxation system (2.4) can be formulated as

$$\begin{cases} \tau_j^{n+1-} = \tau_j^n + \frac{\Delta t}{\Delta m_j}(u^*_{j+\frac{1}{2}} - u^*_{j-\frac{1}{2}}) \\ u_j^{n+1-} = u_j^n - \frac{\Delta t}{\Delta m_j}(\Pi^*_{j+\frac{1}{2}} - \Pi^*_{j-\frac{1}{2}}) - \Delta t\{\frac{g}{\tau}\partial_m z\}_j^n \end{cases} \tag{3.1}$$

where we have set

$$\begin{aligned} u^*_{j+\frac{1}{2}} = u^*_{j+\frac{1}{2}}(\mathbf{Q}_j^n, \mathbf{Q}_{j+1}^n) &= \frac{1}{2}(u_{j+1}^n + u_j^n) - \frac{1}{2a^n_{j+\frac{1}{2}}}(\Pi_{j+1}^n - \Pi_j^n) - \frac{\mathcal{M}^n_{j+1/2}}{2a_{j+1/2}}, \\ \Pi^*_{j+\frac{1}{2}} = \Pi^*_{j+\frac{1}{2}}(\mathbf{Q}_j^n, \mathbf{Q}_{j+1}^n) &= \frac{1}{2}(\Pi_{j+1}^n + \Pi_j^n) - \frac{a^n_{j+\frac{1}{2}}}{2}(u_{j+1}^n - u_j^n), \end{aligned} \tag{3.2}$$

$a^n_{j+\frac{1}{2}} = \max((hc)_j^n, (hc)_{j+1}^n)$, while regarding the source term we have

$$\{\frac{g}{\tau}\partial_m z\}_j^n = \frac{1}{2}\Big(\frac{\Delta m_{j+1/2}}{\Delta m_j}\{\frac{g}{\tau}\partial_m z\}_{j+1/2}^n + \frac{\Delta m_{j-1/2}}{\Delta m_j}\{\frac{g}{\tau}\partial_m z\}_{j-1/2}^n\Big) \quad \text{with} \quad \{\frac{g}{\tau}\partial_m z\}_{j+1/2}^n = \frac{\mathcal{M}^n_{j+1/2}}{\Delta m_{j+1/2}} \quad \forall j \tag{3.3}$$

where $\Delta m_{j+1/2} = (\Delta m_j + \Delta m_{j+1})/2$, $\Delta m_j = \frac{\tau_j^n}{\Delta x}$ and

$$\mathcal{M}_{j+1/2} = \frac{g}{2}(\frac{1}{\tau_j^n} + \frac{1}{\tau_{j+1}^n})(z_{j+1}^n - z_j^n).$$

Let us note that z remains constant in this step, thus $z_j^{n+1-} = z_j^n$ for all j.

Lagrangian reformulation of (3.1). Let us observe that (3.1) reveals to be strictly equivalent to

$$\begin{cases} L_j^{n+1-} h_j^{n+1-} = L_j^n h_j^n \\ L_j^{n+1-}(hu)_j^{n+1-} = L_j^n (hu)_j^n - \frac{\Delta t}{\Delta x}(\Pi^*_{j+\frac{1}{2}} - \Pi^*_{j-\frac{1}{2}}) + \Delta t s_j^n \end{cases} \tag{3.4}$$

where we have set

$$L_j^{n+1-} = L_j^n + \frac{\Delta t}{\Delta x}(u^*_{j+\frac{1}{2}} - u^*_{j-\frac{1}{2}}) \quad \text{with} \quad L_j^n = 1 \tag{3.5}$$

and

$$s = -gh\partial_x z, \quad s_j^n = \frac{1}{2}\Big(s_{j+1/2}^n + s_{j-1/2}^n\Big) \quad \text{and} \quad s_{j+1/2}^n = -\frac{\mathcal{M}^n_{j+1/2}}{\Delta x} \quad \forall j.$$

Considering that the Lagrangian variable ξ is discretized using the same mesh step as the one we used for x, namely $\Delta\xi = \Delta x$, and $\xi_{j+1/2} = x_{j+1/2}$, $\xi_j = x_j$ for all j, it is clear that (3.4) and (3.5) respectively approximate (2.9) and (2.8). This Lagrangian reformulation turns out to be crucial in order to derive hereafter a second-order extension of the propose numerical scheme. Note that we still have of course $z_j^{n+1-} = z_j^n$ for all j.

3.1.2 Projection step

As already mentioned, the aim of this step is to turn into Eulerian coordinates the solution obtained at the end of the previous step thanks to (3.4) and given in Lagrangian coordinates. This amounts to solve the transport system (2.5) which also contains the evolution equation for z. Recall indeed that z stayed constant in the first step.

In order to project $X = h, hu$ on the Eulerian grid, we use the following identity

$$\int_{\xi_1}^{\xi_2} L(\xi,t)X(\xi,t)d\xi = \int_{x(\xi_1,t)}^{x(\xi_2,t)} X(x,t)dx$$

where we recall that the trajectories $t \mapsto x(\xi,t)$ and the volume ratio $L(\xi,t)$ are defined by (2.6) and (2.7). Therefore, it is natural to define $\hat{\xi}_{j+1/2}$ such that $x(\hat{\xi}_{j+1/2}, t^{n+1}) = x_{j+1/2}$ and $x(\hat{\xi}_{j+1/2}, t^n) = \hat{\xi}_{j+1/2}$ for all j and to write

$$X_j^{n+1} = \frac{1}{\Delta x}\int_{x_{j-\frac{1}{2}}}^{x_{j+\frac{1}{2}}} X(x,t^{n+1})dx = \frac{1}{\Delta x}\int_{x(\hat{\xi}_{j-\frac{1}{2}},t^{n+1})}^{x(\hat{\xi}_{j+\frac{1}{2}},t^{n+1})} X(x,t^{n+1})dx = \frac{1}{\Delta x}\int_{\hat{\xi}_{j-\frac{1}{2}}}^{\hat{\xi}_{j+\frac{1}{2}}} L(\xi,t^{n+1-})X(\xi,t^{n+1-})d\xi. \quad (3.6)$$

Splitting the last integral into three parts, namely

$$\begin{aligned} X_j^{n+1} =& \frac{1}{\Delta x}\int_{\hat{\xi}_{j-\frac{1}{2}}}^{\xi_{j-\frac{1}{2}}} L(\xi,t^{n+1-})X(\xi,t^{n+1-})d\xi + \\ &+ \frac{1}{\Delta x}\int_{\xi_{j-\frac{1}{2}}}^{\xi_{j+\frac{1}{2}}} L(\xi,t^{n+1-})X(\xi,t^{n+1-})d\xi + \frac{1}{\Delta x}\int_{\xi_{j+\frac{1}{2}}}^{\hat{\xi}_{j+\frac{1}{2}}} L(\xi,t^{n+1-})X(\xi,t^{n+1-})d\xi, \end{aligned} \quad (3.7)$$

and approximating $\hat{\xi}_{j+1/2}$ by

$$x_{j+1/2} = x(\hat{\xi}_{j+1/2}, t^{n+1}) \simeq x(\hat{\xi}_{j+1/2}, t^n) + \Delta t \partial_t x(\hat{\xi}_{j+1/2}, t^n) \simeq \hat{\xi}_{j+1/2} + \Delta t u^*_{j+1/2},$$

it is natural to set, using first-order approximations of the integrals,

$$X_j^{n+1} = \frac{\xi_{j-\frac{1}{2}} - \hat{\xi}_{j-\frac{1}{2}}}{\Delta x}(LX)_{j-1/2}^{n+1} + (LX)_j^{n+1-} + \frac{\hat{\xi}_{j+\frac{1}{2}} - \xi_{j+\frac{1}{2}}}{\Delta x}(LX)_{j+1/2}^{n+1} \quad (3.8)$$

where for all j

$$(LX)_{j+1/2}^{n+1} = \begin{cases} (LX)_j^{n+1-} & \text{if} \quad u^*_{j+1/2} \geq 0 \\ (LX)_{j+1}^{n+1-} & \text{if} \quad u^*_{j+1/2} < 0. \end{cases}$$

After easy manipulations, (3.8) is equivalent to

$$X_j^{n+1} = (LX)_j^{n+1-} - \frac{\Delta t}{\Delta x}\big(u^*_{j+\frac{1}{2}}(LX)_{j+\frac{1}{2}}^{n+1-} - u^*_{j-\frac{1}{2}}(LX)_{j-\frac{1}{2}}^{n+1-}\big). \quad (3.9)$$

Therefore, taking $X = h$ and $X = hu$ concludes the projection on the Eulerian grid.

Let us now consider the Exner equation for which we propose two different strategies. On one hand, we simply update the topography as in the following

$$z_j^{n+1} = z_j^n - \zeta\frac{\Delta t}{\Delta x}\Big(u^*_{j+\frac{1}{2}}\Big(\frac{q_b}{u}\Big)^n_{j+\frac{1}{2}} - u^*_{j-\frac{1}{2}}\Big(\frac{q_b}{u}\Big)^n_{j-\frac{1}{2}}\Big), \quad (3.10)$$

with

$$(\frac{q_b}{u})^n_{j+1/2} = \begin{cases} (\frac{q_b}{u})(u^n_{j+1}) & \text{if} \quad u^*_{j+\frac{1}{2}} \leq 0 \\ \\ (\frac{q_b}{u})(u^n_j) & \text{if} \quad u^*_{j+\frac{1}{2}} > 0, \end{cases}$$

where we see that the numerical fluxes are evaluated simply using the solution at time t^n, and not the one obtained at the end of the Lagrangian step. This means in some sense that the evolution of the topography is not coupled with the one hydrodynamic model from a numerical point of view and this is the reason why this strategy is said to be *decoupled*. At last, note that $\frac{q_b}{u}$ is well-defined and actually depends on u only, as we suppose the solid transport discharge to be given by the Grass formula with $m_g = 3$. On the other hand, we propose a *weakly coupled* strategy in which we exploit the solution obtained at time t^{n+1-}, by setting

$$z_j^{n+1} = z_j^n - \zeta \frac{\Delta t}{\Delta x}\Big(u^*_{j+\frac{1}{2}}\Big(\frac{q_b}{u}\Big)^{n+1-}_{j+\frac{1}{2}} - u^*_{j-\frac{1}{2}}\Big(\frac{q_b}{u}\Big)^{n+1-}_{j-\frac{1}{2}}\Big). \tag{3.11}$$

At this stage, notice that it would be tempting to define $\Big(\frac{q_b}{u}\Big)^{n+1-}_{j+\frac{1}{2}}$ using the velocity u^{n+1-} simply defined by $u^{n+1-} = \frac{Lhu^{n+1-}}{Lh^{n+1-}}$. However, even if this option results to be natural, dividing by Lh rises difficulties when considering the second-order extension. For this reason, we prefer to set

$$(\frac{q_b}{u})^{n+1-}_{j+1/2} = \begin{cases} (\frac{q_b}{u})\Big((Lu)^{n+1-}_{j+1}\Big) & \text{if} \quad u^*_{j+\frac{1}{2}} \leq 0 \\ \\ (\frac{q_b}{u})\Big((Lu)^{n+1-}_{j}\Big) & \text{if} \quad u^*_{j+\frac{1}{2}} > 0, \end{cases}$$

where a possible discretization of the evolution equation (2.10) for Lu reads

$$(Lu)^{n+1-}_j = (Lu)^n_j + \frac{\Delta t}{2\Delta x}((u^*_{j+\frac{1}{2}})^2 - (u^*_{j-\frac{1}{2}})^2) + \Delta t \frac{\hat{s}_{j+\frac{1}{2}} + \hat{s}_{j-\frac{1}{2}}}{2} \tag{3.12}$$

with

$$\hat{s}_{j+\frac{1}{2}} = -g\frac{(h+z)^n_{j+1} - (h+z)^n_j}{\Delta x}.$$

As a last remark we observe that, since we are also interested in a $2D$ formulation and (2.10) could not be extended in two dimensions as it is (see hereafter), we will propose an alternative approximation of Lu which reads

$$(Lu)^{n+1-}_j = (Lu)^n_j + \frac{u^n_j + u^n_{j+1}}{2}\frac{\Delta t}{\Delta x}(u^*_{j+\frac{1}{2}} - u^*_{j-\frac{1}{2}}) + \Delta t \frac{\hat{s}_{j+\frac{1}{2}} + \hat{s}_{j-\frac{1}{2}}}{2}.$$

Both formulations turn out to give the same results in $1D$.

3.1.3 Overall scheme and well-balanced property

Next, we give an equivalent formulation of our first-order scheme which takes into account both the acoustic and transport steps. This formulation is interesting in the sense that it clearly shows that the scheme is indeed conservative when there is no source term. More precisely, considering together (3.4) and (3.9) we easily get

$$\begin{cases} h^{n+1}_j = h^n_j - \dfrac{\Delta t}{\Delta x}\big(u^*_{j+\frac{1}{2}}(Lh)^{n+1-}_{j+\frac{1}{2}} - u^*_{j-\frac{1}{2}}(Lh)^{n+1-}_{j-\frac{1}{2}}\big) \\ (hu)^{n+1}_j = (hu)^n_j - \dfrac{\Delta t}{\Delta x}\big(u^*_{j+\frac{1}{2}}(Lhu)^{n+1-}_{j+\frac{1}{2}} + \Pi^*_{j+\frac{1}{2}} - u^*_{j-\frac{1}{2}}(Lhu)^{n+1-}_{j-\frac{1}{2}} - \Pi^*_{j-\frac{1}{2}}\big) + \Delta t s^n_j \end{cases} \tag{3.13}$$

while the evolution equations (3.10) and (3.11) for z are clearly conservative. Let us now prove the well-balanced property.

Theorem 1. *The first-order numerical scheme with updating formula (3.13) and (3.10) or (3.11) preserves the "lake at rest" stationary solution (1.6).*

Proof. Assuming to be under the "lake at rest" condition, that is to say $u^n_j = 0$ and $h^n_j + z^n_j =$ constant, for all j, it is straightforward to demonstrate that this stationary solution is preserved. Indeed, few algebraic computations show that $u^*_{j+\frac{1}{2}} = 0$ as $u^n_j = u^n_{j+1} = 0$ and

$$\Pi^n_{j+1} - \Pi^n_j = \frac{g}{2}((h^n_{j+1})^2 - (h^n_j)^2) = \frac{g}{2}(h^n_j + h^n_{j+1})(h^n_{j+1} - h^n_j) = -\frac{g}{2}(h^n_j + h^n_{j+1})(z^n_{j+1} - z^n_j).$$

Similarly, it can be proved that $\frac{1}{\Delta x}(\Pi^*_{j+\frac{1}{2}} - \Pi^*_{j-\frac{1}{2}}) = s^n_j$ and thus $(Lhu)^{n+1-}_j = (Lhu)^n_j = (hu)^n_j = 0$. We can also note that $(Lu)^{n+1-}_j = 0$ as $(h+z)^n_j = (h+z)^n_{j+1}$ for all j. Finally, it is easily seen that under the property $u^*_{j+1/2} = 0$ for all j, then the transport step gives $h^{n+1}_j = h^n_j$, $(hu)^{n+1}_j = 0$, and $z^{n+1}_j = z^n_j$ which concludes the proof. □

3.2 Second-order scheme

We now explain how to reach the second order of accuracy in both space and time. While increasing the order of accuarcy is a standard process, the key issue is to preserve the well-balanced property.

In order to construct a high-order approximation in space, we will make use of classical first-order polynomial reconstructions, but applied to the so-called fluctuations which is non-standard and has been introduced in [40] to combine both the well-balanced property and the higher order property.

Regarding the second-order discretization in time, we simply consider Runge-Kutta TVD scheme at second order [31]. In particular, we apply it to the overall scheme (Lagrangian and remap step together) in order to avoid diffusion due to the splitting.

3.2.1 Lagrangian step

In order to reach the second order of accuracy in space, we begin by defining at time t^n and for each cell j a stationary solution denoted by $x \mapsto \mathbf{Q}^{n,e}_j(x)$ and defined for all x by

$$\big(h^{n,e}_j\big)(x) = h^n_j + z^n_j - z^n(x), \quad u^{n,e}_j(x) = u^n_j \quad \text{and} \quad z^{n,e}_j(x) = z^n(x), \tag{3.14}$$

where $x \mapsto z^n(x)$ is nothing but the piecewise constant approximation of z at time t^n, namely such that $z^n(x) = z^n_j$ for all x in $[x_{j-1/2}, x_{j+1/2})$. Such a reconstructed solution satisfies the in-cell conservativity property

$$\frac{1}{\Delta x}\int_{x_{j-\frac{1}{2}}}^{x_{j+\frac{1}{2}}} \mathbf{Q}^{n,e}_j(x)dx = \mathbf{Q}^n_j.$$

Next, we follow [40] and introduce the so-called j-fluctuations defined as

$$\mathbf{D}^n_{k,j} = \mathbf{Q}^n_k - \frac{1}{\Delta x}\int_{x_{k-1/2}}^{x_{k+1/2}} \mathbf{Q}^{n,e}_j(x)dx,$$

for all k. Observe that $\mathbf{D}^n_{j,j} = \mathbf{0}$ by construction, while $\mathbf{D}^n_{k,j} = \mathbf{0}$ for all k if the approximate solution at time t^n satisfies the "lake at rest" condition (1.6).

At last, for each cell I_j we make use of a reconstructed polynomial vector $\mathbf{P}^n_j(x)$ defined by

$$\mathbf{P}^n_j(x) = \mathbf{Q}^n_j + \Delta^n_j(x - x_j),$$

where $\Delta^n_j = \Delta^n_j(\mathbf{D}^n_{j-1,j}, \mathbf{D}^n_{j,j}, \mathbf{D}^n_{j+1,j})$ is the ENO [46] or the MINMOD [45] slope applied to the fluctuations.

The numerical fluxes $u^*_{j+\frac{1}{2}}$ and $\Pi^*_{j+\frac{1}{2}}$ are then defined in a very classical way using the interfaces values

$$\mathbf{Q}^n_{j+\frac{1}{2}L} = \mathbf{P}^n_j(x_{j+\frac{1}{2}}) \quad \text{and} \quad \mathbf{Q}^n_{j+\frac{1}{2}R} = \mathbf{P}^n_{j+1}(x_{j+\frac{1}{2}}),$$

and formula (3.2), namely

$$u^*_{j+\frac{1}{2}} = u^*_{j+\frac{1}{2}}(\mathbf{Q}^n_{j+\frac{1}{2}L}, \mathbf{Q}^n_{j+\frac{1}{2}R}) \quad \text{and} \quad \Pi^*_{j+\frac{1}{2}} = \Pi^*_{j+\frac{1}{2}}(\mathbf{Q}^n_{j+\frac{1}{2}L}, \mathbf{Q}^n_{j+\frac{1}{2}R}), \tag{3.15}$$

with

$$a^n_{j+\frac{1}{2}} = \max\big(h^n_{j+\frac{1}{2},L}c^n_{j+\frac{1}{2},L}, h^n_{j+\frac{1}{2},R}c^n_{j+\frac{1}{2},R}\big).$$

Regarding the source term, once again we exploit formulas (3.3). Let us note that, thanks to formula (3.14), $z_{j+\frac{1}{2}L} = z_j$ and $z_{j+\frac{1}{2}R} = z_{j+1}$ as the fluctuations related to the topography are null. Finally, the discretization of the Lagrangian system (2.9) reads as in the first-order step, namely

$$\begin{cases} L^{n+1-}_j h^{n+1-}_j = L^n_j h^n_j \\ L^{n+1-}_j (hu)^{n+1-}_j = L^n_j (hu)^n_j - \frac{\Delta t}{\Delta x}(\Pi^*_{j+\frac{1}{2}} - \Pi^*_{j-\frac{1}{2}}) + \Delta t s^n_j. \end{cases}$$

3.2.2 Projection step

In this step, we exploit again a reconstructed polynomial $L\mathbf{P}$. However, in order to preserve the second-order of accuracy, it is crucial to reconstruct the Lagrangian variables (LX), namely as

$$(LX)_j^{n+1-}(\xi) = (LX)_j^{n+1-} + \Delta_j^{n+1-}(\xi - \xi_j) \tag{3.16}$$

with the slope $\Delta_j^{n+1-} = \Delta_j^{n+1-}((LX)_{j-1}^{n+1-}, (LX)_j^{n+1-}, (LX)_{j+1}^{n+1-})$ and where the variable X denotes h, hu and u. Then, the updating formula for $X = h$ and $X = hu$ are given by a second-order approximation of the three integrals that appear in (3.7). This is achieved by using the mid-point rule, thus we get

$$X_j^{n+1-} = (LX)_j^{n+1-} - \frac{\Delta t}{\Delta x}\big(u^*_{j+\frac{1}{2}}(LX)^{n+1-}_{j+\frac{1}{2}}\Big(\frac{\xi_{j+\frac{1}{2}} + \hat{\xi}_{j+\frac{1}{2}}}{2}\Big) - u^*_{j-\frac{1}{2}}(LX)^{n+1-}_{j-\frac{1}{2}}\Big(\frac{\xi_{j-\frac{1}{2}} + \hat{\xi}_{j-\frac{1}{2}}}{2}\Big)\big), \tag{3.17}$$

where we use the upwind definition

$$(LX)^{n+1-}_{j-\frac{1}{2}}(\xi) = \begin{cases} (LX)^{n+1-}_{j-1}(\xi) & \text{if} \quad u^*_{j-\frac{1}{2}} > 0 \\ (LX)^{n+1-}_{j}(\xi) & \text{if} \quad u^*_{j-\frac{1}{2}} \leq 0. \end{cases} \tag{3.18}$$

As far as the topography is concerned, we consider the weakly coupled scheme (3.11) where we naturally set

$$(\frac{q_b}{u})^{n+1-}_{j+1/2} = \begin{cases} (\frac{q_b}{u})\Big((Lu)^{n+1-}_{j+1}(\frac{\xi_{j+\frac{1}{2}} + \hat{\xi}_{j+\frac{1}{2}}}{2})\Big) & \text{if} \quad u^*_{j+\frac{1}{2}} \leq 0 \\ \\ (\frac{q_b}{u})\Big((Lu)^{n+1-}_{j}(\frac{\xi_{j+\frac{1}{2}} + \hat{\xi}_{j+\frac{1}{2}}}{2})\Big) & \text{if} \quad u^*_{j+\frac{1}{2}} > 0, \end{cases}$$

and $u^*_{j\pm\frac{1}{2}}$ is given by (3.15).

Afterwards, for the decoupled scheme, we first define the reconstructed polynomial for the water height h and the flow hu at time t^n,

$$P(X)^n_j(x) = X^n_j + \Delta^n_j(x - x_j)$$

with $X = h, hu$ and Δ^n_j the slopes (either ENO or Minmod). Then, we use formula (3.10) where we impose

$$(\frac{q_b}{u})^{n}_{j+1/2} = \begin{cases} (\frac{q_b}{u})\Big(\frac{P(hu)^n_{j+1}(x_{j+\frac{1}{2}})}{P(h)^n_{j+1}(x_{j+\frac{1}{2}})}\Big) & \text{if} \quad u^*_{j+\frac{1}{2}} \leq 0 \\ \\ (\frac{q_b}{u})\Big(\frac{P(hu)^n_{j}(x_{j+\frac{1}{2}})}{P(h)^n_{j}(x_{j+\frac{1}{2}})}\Big) & \text{if} \quad u^*_{j+\frac{1}{2}} > 0. \end{cases}$$

Theorem 2. *The second-order numerical scheme described preserves the "lake at rest" stationary solution (1.6).*

Proof. Since we already proved the well-balanced property for the first-order scheme, it is straightforward to show it for the second-order method as well. Indeed, it is enough to observe that the slopes $\Delta^n_j = \Delta^n_j(\mathbf{D}^n_{j-1,j}, \mathbf{D}^n_{j,j}, \mathbf{D}^n_{j+1,j})$ are null under the hypothesis of the "lake at rest condition" thanks to definition of the fluctuations. Hence, once again we obtain $u^*_{j+\frac{1}{2}} = 0$ and thus $Lhu^{n+1-}_j = hu^n_j = 0$, $Lh^{n+1-}_j = h^n_j$, $hu^{n+1}_j = Lhu^{n+1-}_j = hu^n_j = 0$, $h^{n+1}_j = Lh^{n+1-}_j = h^n_j$ and $z^{n+1}_j = z^n_j$. Finally, it is only worth to specify that the Runge-Kutta TVD procedure automatically preserves the stationary solutions. □

4 Two-dimensional extension

In this section, we briefly describe how we extend the proposed approach in two space dimensions using dimensional splitting. Let us first recall that if we denote $(x, y) \in \mathbb{R}^2$ the space variables and $\mathbf{u} = (u, v)^T$ the velocity vector, then the

2D shallow water system reads

$$\begin{cases} \partial_t h + \nabla \cdot (h\mathbf{u}) = 0 \\ \partial_t (h\mathbf{u}) + \nabla \cdot (h\mathbf{u} \otimes \mathbf{u}) + \nabla p = -gh\nabla z, \end{cases} \tag{4.1}$$

while the Exner equation is given by

$$\partial_t z + \zeta \partial_x q_{b,x} + \zeta \partial_y q_{b,y} = 0$$

where $q_{b,x}$ and $q_{b,y}$ are the solid transport discharges in the x and y direction respectively. Exploiting once again the Grass model, their formula are the following,

$$q_{b,x} = A_g u(u^2 + v^2) \quad \text{and} \quad q_{b,y} = A_g v(u^2 + v^2).$$

Notice that the "lake at rest" stationary solutions now satisfy

$$u = 0, \quad v = 0 \quad \text{and} \quad \nabla(h + z) = 0.$$

It is still possible to consider a Lagrangian formulation of these equations. More precisely, let us introduce the Lagrangian coordinates (ξ_1, ξ_2) and consider the map : $(\xi_1, \xi_2) \to (x, y)$, with $x = x(\xi_1, \xi_2, t)$, $y = y(\xi_1, \xi_2, t)$ and such that

$$\frac{\partial x}{\partial t} = u(x, y, t) \quad \text{and} \quad \frac{\partial y}{\partial t} = v(x, y, t),$$

$$x(\xi_1, \xi_2, 0) = \xi_1, \quad y(\xi_1, \xi_2, 0) = \xi_2.$$

We also assume that for each $t > 0$, this map is invertible and its Jacobian (determinant of the Jacobian matrix) is given by

$$L(\xi_1, \xi_2, t) = \begin{vmatrix} \partial_{\xi_1} x & \partial_{\xi_2} x \\ \partial_{\xi_1} y & \partial_{\xi_2} y \end{vmatrix}$$

with $L(\xi_1, \xi_2, 0) = 1$ and, after easy calculations,

$$\frac{\partial L(\xi_1, \xi_2, t)}{\partial t} = L\nabla \cdot \mathbf{u} = L\partial_x u + L\partial_y v. \tag{4.2}$$

Then, it can be shown that the Lagrangian formulation of the system writes

$$\begin{cases} \partial_t (Lh) = 0 \\ \partial_t (Lh\mathbf{u}) + L\nabla p = -ghL\nabla z, \end{cases} \tag{4.3}$$

where the gradient is still taken with respect to the Eulerian variables (x, y), while on the other hand we also have

$$\partial_t (L\mathbf{u}) - \mathbf{u}L\nabla \cdot \mathbf{u} + gL\nabla(h + z) = 0,$$

which will be useful hereafter. We refer the reader to [35, 37] for more details about Lagrangian coordinates in $2-$dimensions.

We now give the basic formulas based on a dimensional splitting and introduce some notations. First of all, the computational domain $\Omega \subset \mathbb{R}$ is divided into $M_x \times M_y$ rectangular cells with constant space steps Δx and Δy in the x and y directions respectively. Then, the mesh interfaces are given by $x_{i+1/2}$ for $i \in \{0, \dots, M_x\}$ and $y_{j+1/2}$ for $j \in \{0, \dots, M_y\}$. Thus, $\varphi_{i,j}^n$ denotes the piecewise constant approximation of the variable φ in the cell $[x_{i-1/2}, x_{i+1/2}) \times [y_{j-1/2}, y_{j+1/2})$ at time t^n, namely

$$\varphi_{i,j}^n \approx \frac{1}{\Delta x} \int_{x_{i-1/2}}^{x_{i+1/2}} \int_{y_{j-1/2}}^{y_{j+1/2}} \varphi(x, y, t^n)\, dx\, dy.$$

Acoustic step

Following the 1D scheme, the numerical approximation of (4.3) is taken to be

$$\begin{cases} (Lh)_{i,j}^{n+1-} = (Lh)_{i,j}^{n} \\ (Lhu)_{i,j}^{n+1-} = (Lhu)_{i,j}^{n} - \dfrac{\Delta t}{\Delta x}(\Pi^*_{i+\frac{1}{2},j} - \Pi^*_{i-\frac{1}{2},j}) + \Delta t s_{i,j}^{1,n} \\ (Lhv)_{i,j}^{n+1-} = (Lhv)_{i,j}^{n} - \dfrac{\Delta t}{\Delta y}(\Pi^*_{i,j+\frac{1}{2}} - \Pi^*_{i,j-\frac{1}{2}}) + \Delta t s_{i,j}^{2,n} \end{cases} \tag{4.4}$$

where we have set

$$L_{i,j}^{n+1-} = L_{i,j}^{n} + \frac{\Delta t}{\Delta x}(u^*_{i+\frac{1}{2},j} - u^*_{i-\frac{1}{2},j}) + \frac{\Delta t}{\Delta y}(v^*_{i,j+\frac{1}{2}} - v^*_{i,j-\frac{1}{2}}) \tag{4.5}$$

with

$$\begin{aligned} u^*_{i+\frac{1}{2},j} &= \frac{1}{2}(u^n_{i+1,j} + u^n_{i,j}) - \frac{1}{2a^n_{i+\frac{1}{2},j}}(\Pi^n_{i+1,j} - \Pi^n_{i,j}) - \frac{\mathcal{M}^n_{i+1/2,j}}{2a_{i+1/2,j}}, \\ v^*_{i,j+\frac{1}{2}} &= \frac{1}{2}(v^n_{i,j+1} + v^n_{i,j}) - \frac{1}{2a^n_{i,j+\frac{1}{2}}}(\Pi^n_{i,j+1} - \Pi^n_{i,j}) - \frac{\mathcal{M}^n_{i,j+1/2}}{2a_{i,j+1/2}}, \\ \Pi^*_{i+\frac{1}{2},j} &= \frac{1}{2}(\Pi^n_{i+1,j} + \Pi^n_{i,j}) - \frac{a^n_{i+\frac{1}{2},j}}{2}(u^n_{i+1,j} - u^n_{i,j}), \\ \Pi^*_{i,j+\frac{1}{2}} &= \frac{1}{2}(\Pi^n_{i,j+1} + \Pi^n_{i,j}) - \frac{a^n_{i,j+\frac{1}{2}}}{2}(v^n_{i,j+1} - v^n_{i,j}), \end{aligned} \tag{4.6}$$

with $a^n_{i+1/2,j} = \max((hc)^n_{i,j}, (hc)^n_{i+1,j})$, $a^n_{i,j+1/2} = \max((hc)^n_{i,j}, (hc)^n_{i,j+1})$, while regarding the source term we have for all j

$$\begin{aligned} s^{1,n}_{i,j} &= \frac{1}{2}\Big(s^n_{i+1/2,j} + s^n_{i-1/2,j}\Big) \quad \text{with} \quad s^n_{i+1/2,j} = -\frac{\mathcal{M}^n_{i+1/2,j}}{\Delta x} \\ s^{2,n}_{i,j} &= \frac{1}{2}\Big(s^n_{i,j+1/2} + s^n_{i,j-1/2}\Big) \quad \text{with} \quad s^n_{i,j+1/2} = -\frac{\mathcal{M}^n_{i,j+1/2}}{\Delta y} \end{aligned}$$

with

$$\mathcal{M}^n_{i+1/2,j} = \frac{g}{2}(\frac{1}{\tau^n_{i,j}} + \frac{1}{\tau^n_{i+1,j}})(z^n_{i+1,j} - z^n_{i,j}), \quad \mathcal{M}^n_{i,j+1/2} = \frac{g}{2}(\frac{1}{\tau^n_{i,j}} + \frac{1}{\tau^n_{i,j+1}})(z^n_{i,j+1} - z^n_{i,j}).$$

It is clear that the numerical scheme (4.6) is a natural extension of the one used for the one-dimensional system.

Projection step

As before, the second step of the Lagrange-projection scheme consists in projecting the solution obtained at the end of the acoustic step onto the Eulerian grid, that is to say in approximating the transport system

$$\partial_t \varphi + \mathbf{u} \cdot \nabla \varphi = 0$$

or equivalently

$$\partial_t \varphi + \nabla \cdot (\varphi \mathbf{u}) - \varphi \nabla \cdot \mathbf{u} = 0,$$

where we assumed $\varphi = h, hu, hv$. Here and analogously to the 1D formulation (3.9), we simply set

$$\varphi^{n+1}_{i,j} = (L\varphi)^{n+1-}_{i,j} - \frac{\Delta t}{\Delta x}\Big(u^*_{i+\frac{1}{2},j}(L\varphi)^{n+1-}_{i+\frac{1}{2},j} - u^*_{i-\frac{1}{2},j}(L\varphi)^{n+1-}_{i-\frac{1}{2},j}\Big) - \frac{\Delta t}{\Delta y}\Big(v^*_{i,j+\frac{1}{2}}(L\varphi)^{n+1-}_{i,j+\frac{1}{2}} - v^*_{i,j-\frac{1}{2}}(L\varphi)^{n+1-}_{i,j-\frac{1}{2}}\Big), \tag{4.7}$$

where

$$(L\varphi)^{n+1-}_{i-\frac{1}{2},j} = \begin{cases} (L\varphi)^{n+1-}_{i-1,j} & \text{if} \quad u^*_{i-\frac{1}{2},j} > 0 \\ (L\varphi)^{n+1-}_{i,j} & \text{if} \quad u^*_{i-\frac{1}{2},j} \le 0, \end{cases} \quad \text{and} \quad (L\varphi)^{n+1-}_{i,j-\frac{1}{2}} = \begin{cases} (L\varphi)^{n+1-}_{i,j-1} & \text{if} \quad v^*_{i,j-\frac{1}{2}} > 0 \\ (L\varphi)^{n+1-}_{i,j} & \text{if} \quad v^*_{i,j-\frac{1}{2}} \le 0. \end{cases}$$

The Exner equation. As a natural extension of (3.11), we set

$$z_{i,j}^{n+1} = z_{i,j}^n - \zeta \frac{\Delta t}{\Delta x}\Big(u^*_{i+\frac12,j}\Big(\frac{q_{b,x}}{u}\Big)^{n+1-}_{i+\frac12,j} - u^*_{i-\frac12,j}\Big(\frac{q_{b,x}}{u}\Big)^{n+1-}_{i-\frac12,j}\Big) - \zeta\frac{\Delta t}{\Delta y}\Big(v^*_{i,j+\frac12}\Big(\frac{q_{b,y}}{v}\Big)^{n+1-}_{i,j+\frac12} - v^*_{i,j-\frac12}\Big(\frac{q_{b,y}}{v}\Big)^{n+1-}_{i,j-\frac12}\Big)$$

with

$$(\frac{q_{b,x}}{u})^{n+1-}_{i+1/2,j} = \begin{cases} (\frac{q_{b,x}}{u})\Big((L\mathbf{u})^{n+1-}_{i+1,j}\Big) & \text{if} \quad u^*_{i+1/2,j} \le 0 \\ (\frac{q_{b,x}}{u})\Big((L\mathbf{u})^{n+1-}_{i,j}\Big) & \text{if} \quad u^*_{i+1/2,j} > 0, \end{cases} \quad \text{and} \quad (\frac{q_{b,y}}{v})^{n+1-}_{i,j+1/2} = \begin{cases} (\frac{q_{b,y}}{v})\Big((L\mathbf{u})^{n+1-}_{i,j+1}\Big) & \text{if} \quad v^*_{i,j+1/2} \le 0 \\ (\frac{q_{b,y}}{v})\Big((L\mathbf{u})^{n+1-}_{i,j}\Big) & \text{if} \quad v^*_{i,j+1/2} > 0, \end{cases}$$

where a possible discretization of the evolution equations for Lu and Lv read

$$(Lu)^{n+1-}_{i,j} = (Lu)^n_{i,j} + \Delta t \frac{u_{i+1,j}+u_{i,j}}{2}\big(\frac{1}{\Delta x}(u^*_{i+\frac12,j} - u^*_{i-\frac12,j}) + \frac{1}{\Delta y}(v^*_{i,j+\frac12} - v^*_{i,j-\frac12})\big) - \Delta t \frac{\hat s_{i+\frac12,j} + \hat s_{i-\frac12,j}}{2}$$

and

$$(Lv)^{n+1-}_{i,j} = (Lv)^n_{i,j} + \Delta t \frac{v_{i,j+1}+v_{i,j}}{2}\big(\frac{1}{\Delta x}(u^*_{i+\frac12,j} - u^*_{i-\frac12,j}) + \frac{1}{\Delta y}(v^*_{i,j+\frac12} - v^*_{i,j-\frac12})\big) - \Delta t \frac{\hat s_{i,j+\frac12} + \hat s_{i,j-\frac12}}{2}$$

where $\hat s_{i+\frac12,j} = g((h+z)_{i+1,j} - (h+z)_{i,j})/\Delta x$ and $\hat s_{i,j+\frac12} = g((h+z)_{i,j+1} - (h+z)_{i,j})/\Delta y$.

2D extension of the second-order scheme

We now briefly discuss the extension of the second-order scheme, distinguishing among the Exner equation and the Lagrangian and projection steps for the shallow water system. Once again we reach the second order of accuracy in time exploiting the Runge-Kutta procedure, which is applied to the Lagrangian and projection step together. As expected, the overall strategy is analogous to what we have done for the 1D case.

Regarding the Lagrangian step, we proceed as usual and compute the numerical fluxes $u^*_{i+\frac12,j}$, $v^*_{i,j+\frac12}$, $\Pi^*_{i+\frac12,j}$ and $\Pi^*_{i,j+\frac12}$, but also the speeds $a_{i+1/2,j}$ and $a_{i,j+1/2}$ using left and right interfaces values defined by means of reconstructed polynomials as in the 1D case, namely

$$\mathbf{V}^n_{i+1/2L,j} = \mathbf{V}^n_{i,j} + \Delta^{x,t}_{i,j}\frac{\Delta x}{2}, \quad \mathbf{V}^n_{i+1/2R,j} = \mathbf{V}^n_{i+1,j} - \Delta^{x,t}_{i+1,j}\frac{\Delta x}{2} \tag{4.8}$$

in the x direction, and

$$\mathbf{V}^n_{i,j+1/2L} = \mathbf{V}^n_{i,j} + \Delta^{y,t}_{i,j}\frac{\Delta y}{2}, \quad \mathbf{V}^n_{i,j+1/2R} = \mathbf{V}^n_{i,j+1} - \Delta^{y,t}_{i,j+1}\frac{\Delta y}{2} \tag{4.9}$$

along the y axis, where we have set $\mathbf{V} = (h, hu, hv)^T$. At this stage, we only need to define the slopes $\Delta^{x,t}_{i,j}$, $\Delta^{y,t}_{i,j}$ which are computed exactly as in the 1D case thanks to the definition of fluctuations in the x, respectively y, direction and considering that the $y = y_j$, resp. $x = x_i$, is fixed and using reconstructed stationary solutions direction by direction. The details are left to the reader. In particular, such a strategy guarantees the well-balanced property of the numerical scheme, since the slopes turn out to be null under the "lake at rest" conditions.

Regarding the transport step, we consider a direct 2D extension of (3.17) namely

$$\begin{aligned} X^{n+1}_{i,j} =& (LX)^{n+1-}_{i,j} - \frac{\Delta t}{\Delta x}\Big(u^*_{i+\frac12,j}(LX)^{n+1-}_{i+\frac12,j}\Big(\frac{\xi_{1,i+\frac12} + \hat\xi_{1,i+\frac12}}{2}\Big) - u^*_{i-\frac12,j}(LX)^{n+1-}_{i-\frac12,j}\Big(\frac{\xi_{1,i-\frac12} + \hat\xi_{1,i-\frac12}}{2}\Big)\Big) \\ & - \frac{\Delta t}{\Delta y}\Big(v^*_{i,j+\frac12}(LX)^{n+1-}_{i,j+\frac12}\Big(\frac{\xi_{2,j+\frac12} + \hat\xi_{2,j+\frac12}}{2}\Big) - v^*_{i,j-\frac12}(LX)^{n+1-}_{i,j-\frac12}\Big(\frac{\xi_{2,j-\frac12} + \hat\xi_{2,j-\frac12}}{2}\Big)\Big), \end{aligned}$$

where we have used clear notations which are based on classical first-order polynomial reconstructions of the Lagrangian unknowns (LX) in each direction as in the 1D case, with $X = h, hu, hv$.

Finally, exploiting also the reconstructed values for Lu and Lv and using again classical notations, we suggest a direct 2D extension of (3.11) namely

$$z_{i,j}^{n+1} = z_{i,j}^{n} - \zeta \frac{\Delta t}{\Delta x}\Big(u_{i+1/2,j}^{*}\Big(\frac{q_{b,x}}{u}\Big)_{i+1/2,j}^{n+1-} - u_{i-1/2,j}^{*}\Big(\frac{q_{b,x}}{u}\Big)_{i-1/2,j}^{n+1-}\Big) - \zeta \frac{\Delta t}{\Delta y}\Big(v_{i,j+1/2,}^{*}\Big(\frac{q_{b,y}}{v}\Big)_{i,j+1/2}^{n+1-} - u_{i,j-1/2}^{*}\Big(\frac{q_{b,y}}{v}\Big)_{i,j-1/2}^{n+1-}\Big)$$

with a natural definition for the numerical fluxes $\frac{q_{b,x}}{u}$ and $\frac{q_{b,y}}{v}$. Again, the details are left to the reader since there is no ambiguity.

To conclude this 2D section, let us mention that both the schemes described here preserve the "lake at rest" stationary solutions. The proof is analogous to the one seen in 1D.

5 Numerical results

This section is devoted to the presentation of the simulations and outputs of the numerical schemes we described so far. Regarding the 1D time step value, at each time t^n we compute two different time steps, one for the acoustic system and the other for the transport part, which respectively read

$$\Delta t \leq \text{CFL}_l \frac{\Delta x}{\max\limits_j\{\max(\tau_j^n, \tau_{j+1}^n) a_{j+\frac{1}{2}}\}},$$

and

$$\Delta t \leq \text{CFL}_t \frac{\Delta x}{\max\limits_j\{u_{j-\frac{1}{2}}^{+} - u_{j+\frac{1}{2}}^{-}\}},$$

where CFL_l and CFL_t are respectively the CFL number for the Lagrangian and the transport system, and

$$u_{j-\frac{1}{2}}^{+} = \max(u_{j-\frac{1}{2}}^{*}, 0) \quad \text{and} \quad u_{j+\frac{1}{2}}^{-} = \min(u_{j+\frac{1}{2}}^{*}, 0).$$

Then, the final time step is taken as the minimum between the two. If working in 2D, the acoustic time step is automatically extended, it is enough to consider both directions, while the transport time step reads

$$\Delta t \leq \text{CFL}_t \min_{i,j}\Big\{\Big\{\frac{u_{i-\frac{1}{2},j}^{+} - u_{i+\frac{1}{2},j}^{-}}{\Delta x} + \frac{v_{i,j-\frac{1}{2}}^{+} - v_{i,j+\frac{1}{2}}^{-}}{\Delta y}\Big\}^{-1}\Big\}.$$

Finally, if not otherwise specified, we take $\zeta = 1$, $q_b = A_g u^3$ with $A_g = 0.005$ for the Exner equation, and transmissive boundary conditions. For the CFL number we use $\text{CFL}_l = 0.45$ and $\text{CFL}_l = 0.25$ for the first and second order schemes respectively, while $\text{CFL}_t = 1$. When the 1D reference solution is inserted, it is computed exploiting the second-order scheme with decoupled approximation (3.10) for the Exner equation. Then, $M = 2000$ cells are used, where $\Delta x = \frac{L}{M}$ with L the length of the channel.

5.1 Test of order of accuracy

Here we test the order of accuracy of the numerical schemes described previously. Let us consider a channel of length $L = 20m$, $A_g = 0.3$, $m = 3$. The initial condition is given by null velocity and

$$\begin{cases} z_{IC} = 0.1 - 0.01e^{-(x-10)^2} \\ h_{IC} = 2 - 0.1e^{-(x-10)^2}. \end{cases}$$

We refer to paper [10] for this test case. The reference solution is computed using $M = 4096$ cells and second order decoupled method. In table 1 we inserted the error in norm $\mathbf{L}^1$ and the empirical order of accuracy (EOA) for the water height h, the discharge q and the topography z of both the weakly coupled and decoupled approach. We can see that both schemes reach the second order of accuracy as expected.

Method	Mesh M	Variable	err $\mathbf{L}^1$	$O(\mathbf{L}^1)$	Variable	err $\mathbf{L}^1$	$O(\mathbf{L}^1)$	Variable	err $\mathbf{L}^1$	$O(\mathbf{L}^1)$
Decoupled	64	h	0.0268	–	hu	0.1175	–	z	0.1792×10^{-3}	–
	128		0.0083	1.6953		0.0354	1.7320		0.0544×10^{-3}	1.7190
	256		0.0027	1.6185		0.0115	1.6249		0.0182×10^{-3}	1.5785
	512		0.0007	1.8756		0.0031	1.8782		0.0050×10^{-3}	1.8761
	1024		0.0002	1.9781		0.0008	1.9818		0.0012×10^{-3}	1.9932
Weakly coupled	64	h	0.0268	–	hu	0.1175	–	z	0.1824×10^{-3}	–
	128		0.0083	1.6955		0.0354	1.7320		0.0550×10^{-3}	1.7296
	256		0.0027	1.6182		0.0115	1.6248		0.0183×10^{-3}	1.5890
	512		0.0007	1.8755		0.0031	1.8781		0.0050×10^{-3}	1.8734
	1024		0.0002	1.9782		0.0008	1.9818		0.0013×10^{-3}	1.9792

Table 1: Errors and empirical convergence rates for norm $\mathbf{L}^1$. Mesh of size $M = (64, 128, 256, 512, 1024, 2048)$, $CFL = 0.25$. Second-order decoupled and weakly coupled numerical schemes.

5.2 1D Riemann problem: dam break on movable bottom

For this Riemann problem we refer to [2]. The length of the channel is $L = 10m$ and the dam is placed in the middle. The ending time is $t_{end} = 1s$. The initial condition is given by null velocity, flat topography and water height $h_L = 2m$ if $x < L/2$, $h_R = 0.125m$ if $x > L/2$. In figure 1 we insert the numerical results given by the first-order weakly coupled scheme exploiting two different meshes, in particular $M = 200$ and $M = 2000$ cells. In the second case, we observe that the first-order solution converges towards the reference one, while for $M = 200$ the solution is less accurate in the plateau zone when considering the topography z. On the other hand, no spurious oscillations appear.

Next, in figure 2, we insert the results for the decoupled and weakly coupled second order numerical methods for different mesh sizes, $M = 100$, $M = 200$ and $M = 500$ cells . These two schemes give similar results and, in the topography outputs of both of them, we note some oscillations which decrease as we refine the mesh. We also observe that these oscillations are more accentuated in the decoupled scheme outputs. This is indeed expected as in the decoupled scheme the topography is not coupled with the hydrodynamic model.

5.3 1D sub-critical and supercritical regions

For the following two numerical tests we refer to paper [26]. As initial condition we consider the sub-critical steady state

$$\begin{cases} hu(x, t = 0) = 0.5 \\ z(x, t = 0) = 0.1(1 + e^{-(x-5)^2}) \\ \frac{u^2}{2} + g(h + z) = 6.386, \end{cases}$$

while the length of the channel is $L = 10.0m$. In figure 3 we insert the results of the first and second-order numerical schemes computed with $M = 200$. We consider both $A_g = 0.005$ (top) and $A_g = 0.07$ (bottom). In both cases, the results are satisfying. In work [26], the authors noted as a splitting numerical scheme could produce oscillations in the solution of this numerical test, but to reduce the CFL number could remedy the problem. By splitting numerical scheme, they mean a method which solves before the shallow water system for a fixed topography, and then update the bed level according to the Exner equation. For our method it is not necessary to further decrease the CFL due to the Lagrange-projection splitting whose numerical diffusion is sufficient as coming from both steps. Then, in the same paper [26], the authors presented another test case in which the oscillations of the numerical solution of the splitting method could not be removed, even reducing the CFL number. In figure 4 we show that our solution does not present any oscillation. The decoupled method outputs are not reported as they are very close to the weakly coupled ones. For this last test case, the coefficient A_g is kept null until time $t = 15s$ is reached, then the value $A_g = 0.0005$ is used. As IC we considered

$$\begin{cases} hu(x, t = 0) = 0.6 \\ z(x, t = 0) = 0.1(1 + e^{-(x-5)^2}) \\ h(x, t = 0) + z(x, t = 0) = 0.4. \end{cases}$$

Note that in this test case we have both sub-critical and supercritical regions.

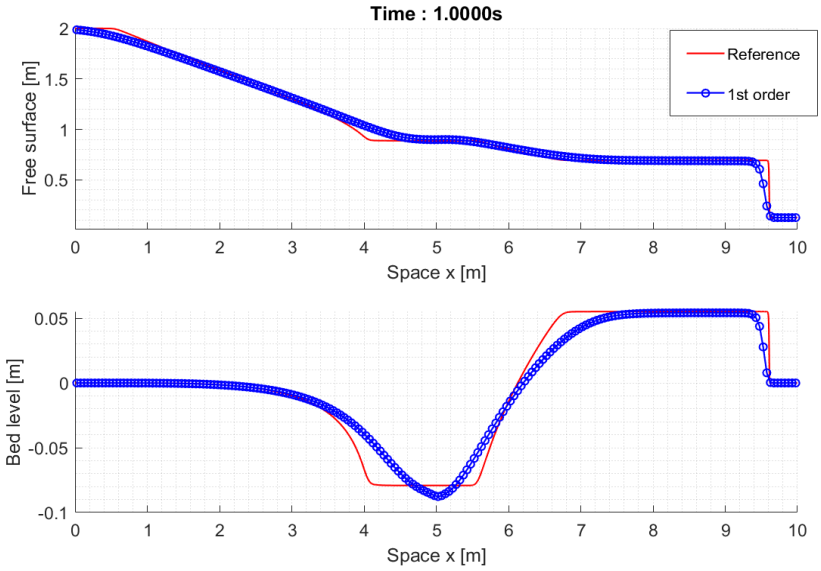

(a) $M = 200$ cells

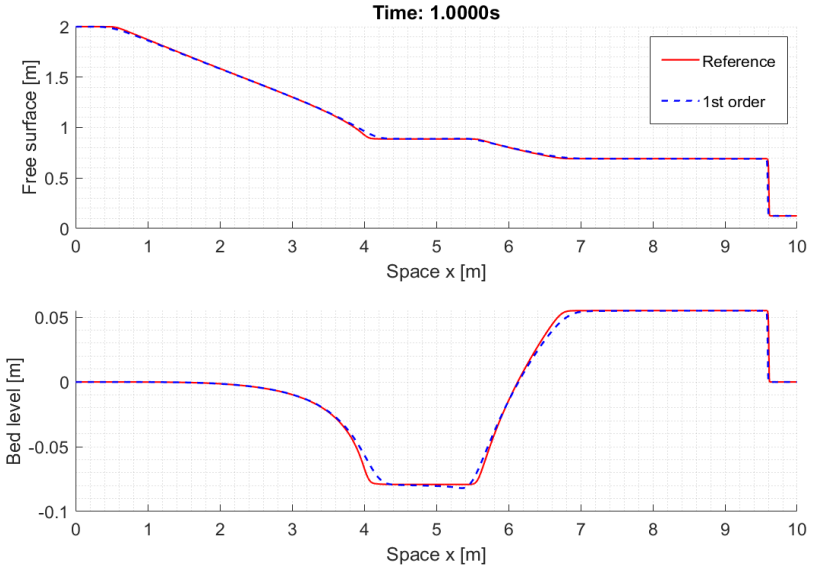

(b) $M = 2000$ cells

Figure 1: RP: dam break on movable bottom; free surface (up) and bed level (bottom). Reference solution (red) and first-order weakly coupled solution (blue). $M = 200$ cells (up) and $M = 2000$ cells (bottom).

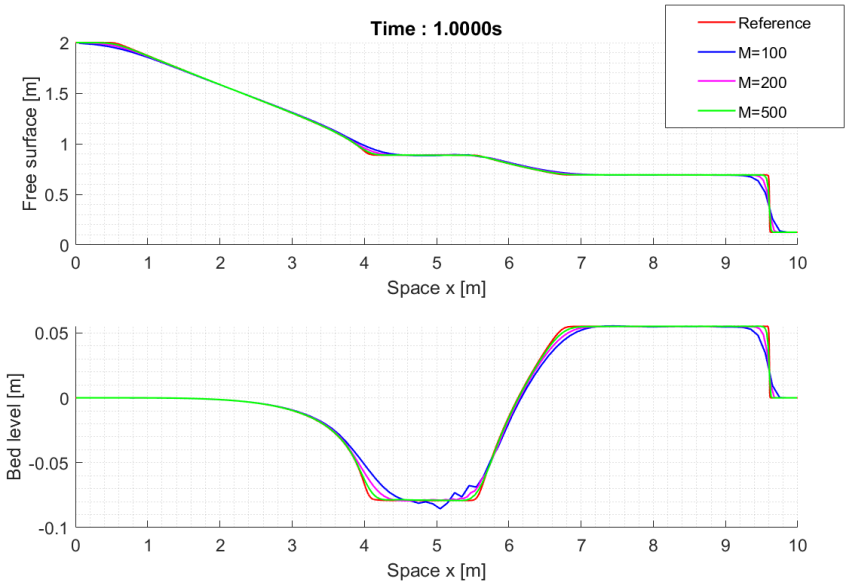

(a) 2nd order weakly coupled scheme

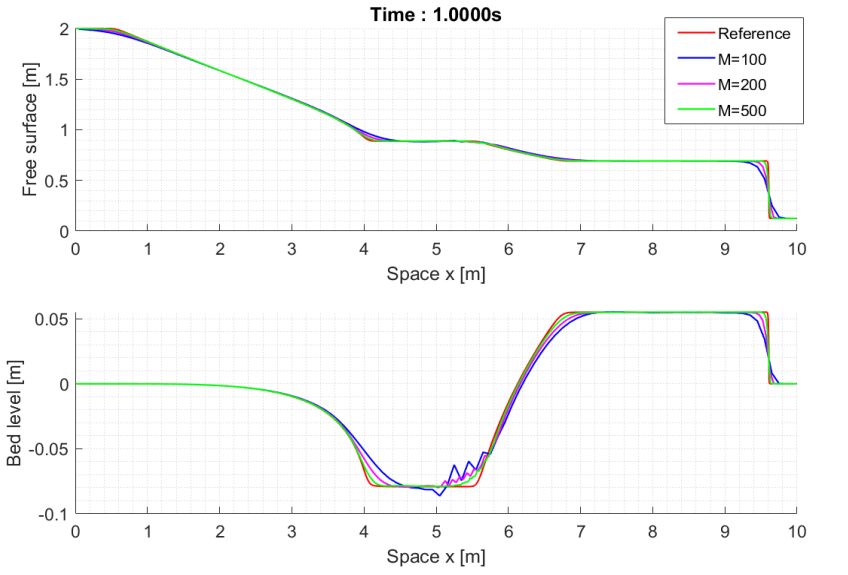

(b) 2nd order decoupled scheme

Figure 2: RP: dam break on movable bottom; free surface (up) and bed level (bottom). "Decoupled" (bottom) and "weakly coupled" (up) solutions. Mesh of size $M = 100$ (blue line), $M = 200$ (magenta line) and $M = 500$ (green line) cells. Red line for reference solution.

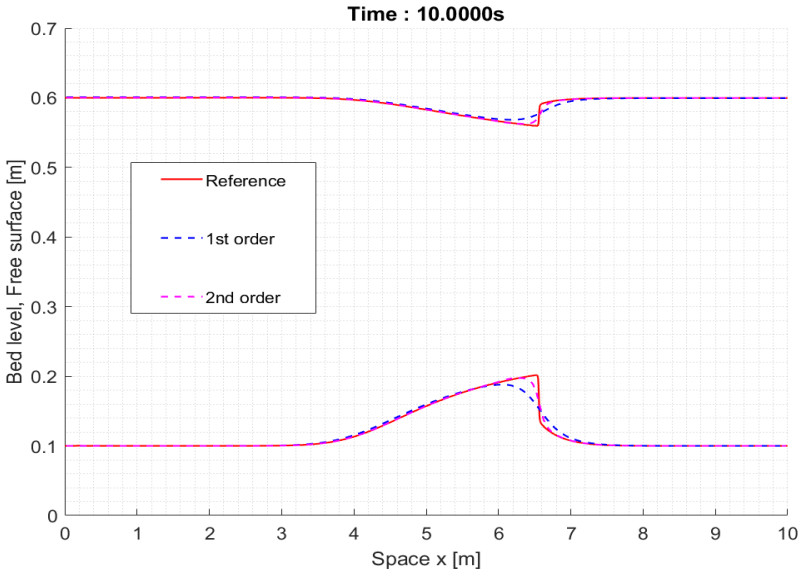

(a) $A_g = 0.005$

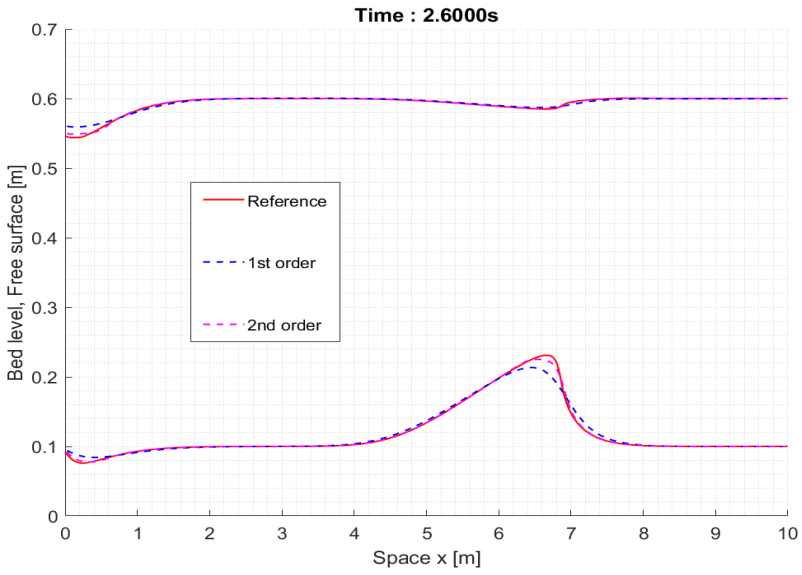

(b) $A_g = 0.07$

Figure 3: Flow over a movable bump; bed level z and free surface $z + h$. First (blue) and second-order (magenta) weakly coupled solutions with $M = 200$ cells. Reference solution in red.

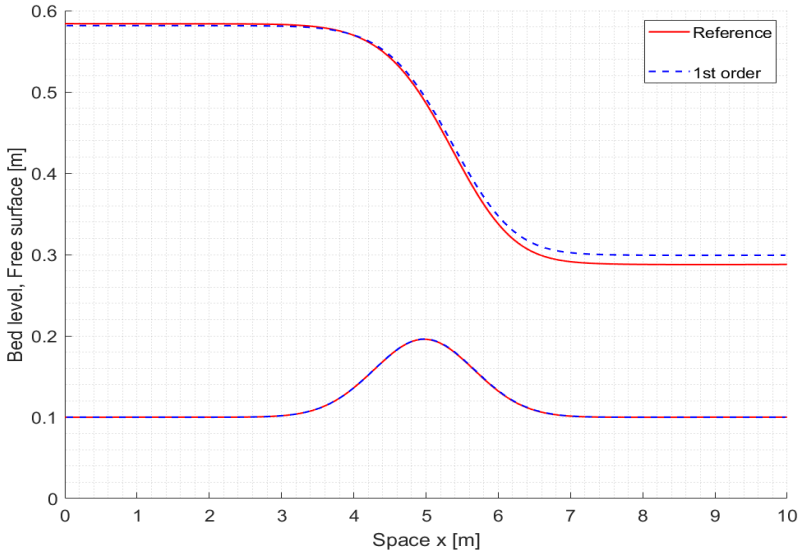

(a) $t_{end} = 16.2s$

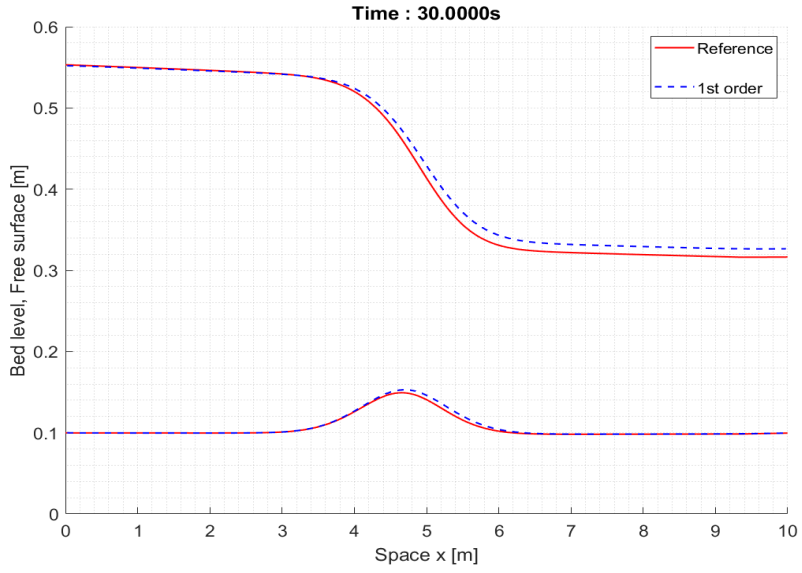

(b) $t_{end} = 30s$

Figure 4: Free surface and bed level, $M = 200$ cells. Reference solution (red) and first-order weakly coupled solution (blue).

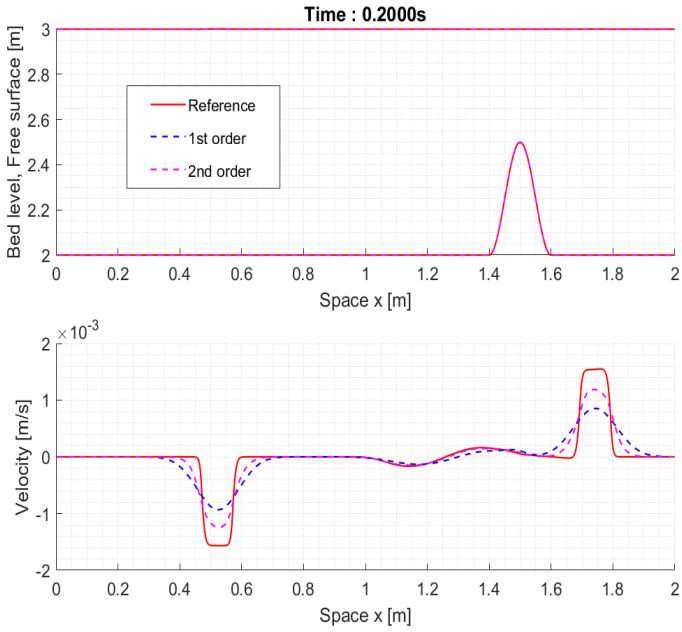

Figure 5: Propagation of perturbation; bed level z and free surface $z + h$ (top), velocity (bottom). First (blue) and second-order (magenta) weakly coupled solutions with $M = 200$ cells. Reference solution in red.

5.4 1D "lake at rest" solution and perturbation

This numerical test is useful to check the well-balanced property of the numerical scheme as we start considering a stationary solution and then we insert some perturbations. For the numerical tests of this section, see [22]. Thus, let us consider as initial condition null velocity, $h(x, t = 0) + z(x, t = 0) = 3m$ and

$$z(x, t = 0) = \begin{cases} 2 + 0.25(cos(10\pi(x - 0.5)) + 1) & \text{if} \quad 1.4 < x < 1.6 \\ 2 & \text{otherwise.} \end{cases}$$

The length of the channel is $L = 2.0m$. Both first and second-order schemes maintain the steady state up to an error of order 10^{-15}.

As a second step, let us introduce small perturbations, namely we impose

$$h(x, t = 0) = \begin{cases} 3 - z(x, t = 0) + 0.001 & \text{if} \quad 1.1 < x < 1.2 \\ 3 - z(x, t = 0) & \text{otherwise.} \end{cases}$$

In figure 5 we compare the results of first and second order numerical schemes against the reference solution. We observe that the outputs are satisfying and in agreement with the ones showed in work [22], no spurious oscillations appear. Clearly, the second order results are less diffusive than the first-order one.

5.5 Circular dam break on wet bed

Let us now consider test problems in 2 dimensions. In this first simple test, the Exner equation is not taken into account, refer to [44]. The domain is a $L \times L$ square with $L = 50$m. Here as initial condition we consider a flat topography, null velocities in both the x and y directions and water height

$$h(x, y, t = 0) = \begin{cases} 10 & \text{if} \quad r \leq 11\text{m} \\ 1 & \text{if} \quad r > 11\text{m}, \end{cases}$$

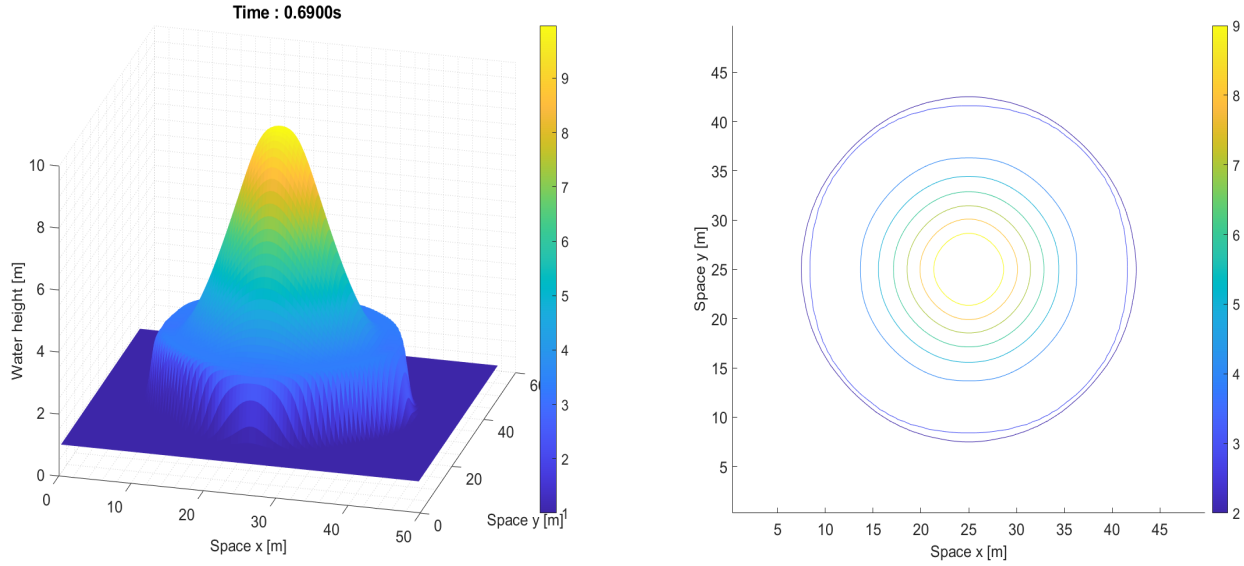

Figure 6: 2D circular dam break on wet bed; water height (left) and its contour plot (right). 2D extension of first-order scheme solution. $M = 100$ cells, $t_{\text{End}} = 0.69$s and CFL$= 0.45$.

with $r = \sqrt{(x-25)^2 + (y-25)^2}$. Thus, we are considering a cylindrical dam that instantaneously breaks at the beginning time $t = 0$s. The ending time $t_{\text{End}} = 0.69$s. Satisfying results of the first order scheme are reported in figure 6.

5.6 Water drop in a basin

For this numerical test, see [4]. Here we simulate a water drop in a basin and consequently reflective boundary conditions are used. A L-side square domain with $L = 20$m is considered. The topography is still taken flat and constant in time. At initial time we assume $\mathbf{u} = (0, 0)^t$ and

$$h(x, y, t = 0) = 2.4(1 + e^{-0.25((x-10.05)^2+(y-10.05)^2)})$$

The outputs are shown in figure 7 at time $t = 1$s, $t = 2$s, $t = 3$s and $t = 4$s respectively. The results agree with the ones reported in [4]. In particular, in the same picture 7, we compare the results at time $t = 4$s obtained using the 2D extensions of the first-order and second-order schemes. We can clearly see that the latter scheme gives less diffusive solutions under the same mesh $M = 100$ cells.

5.7 2D squared dam break

Once again we assume flat topography constant in time. The domain is a square of side $L = 200$m. The dam position is represented in figure 8. We note a breach of length 75m which is instantaneously opened at time $t = 0$. At initial time we also have null velocities and

$$h(x, y, t = 0) = \begin{cases} 10 & \text{if} \quad x \leq 100\text{m} \\ 5 & \text{if} \quad x > 100\text{m}. \end{cases}$$

For more details refer to paper [44]. The results for the water height and the velocity field are shown in figure 9 and they appear to be in agreement with the reference outputs given in [44].

5.8 2D flow over a smooth bump

The following test problem is useful to check the well-balanced property of the scheme, see [44]. The domain is a square of side $L = 1$m and we consider the Grass formulation for the Exner equation with $A_g = 1$ and $\zeta = 1$. At initial time we

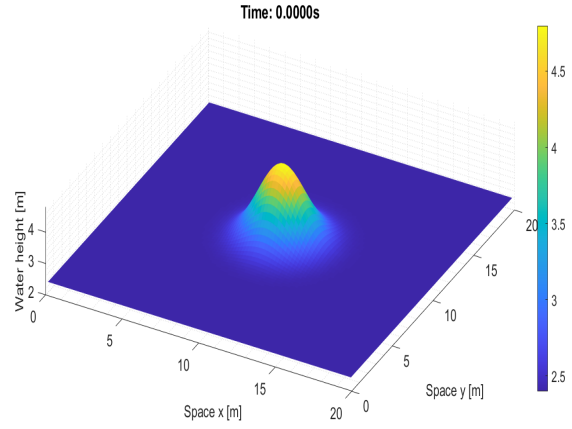

(a) $t = 0$s, 2D extension of 2nd-order scheme

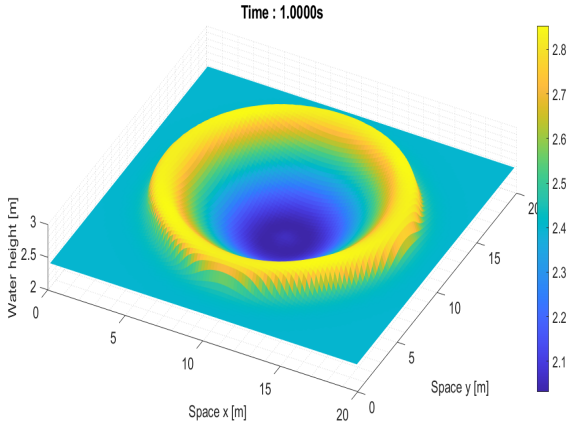

(b) $t = 1$s, 2D extension of 2nd-order scheme

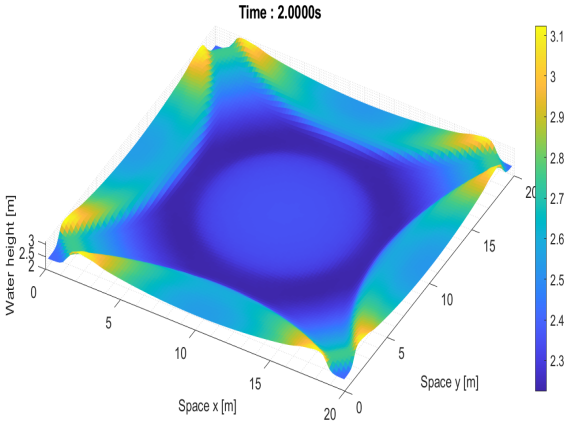

(c) $t = 2$s, 2D extension of 2nd-order scheme

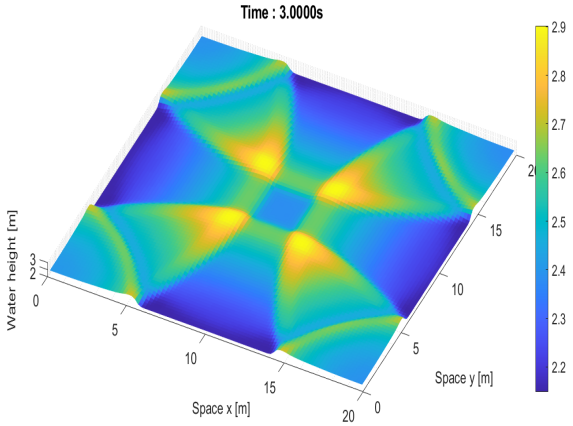

(d) $t = 3$s, 2D extension of 2nd-order scheme

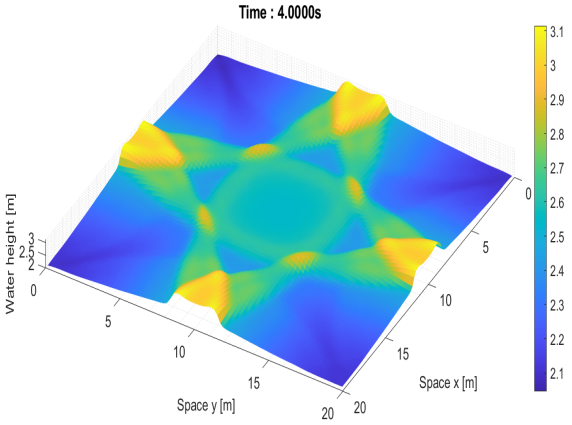

(e) $t = 4$s, 2D extension of 2nd-order scheme

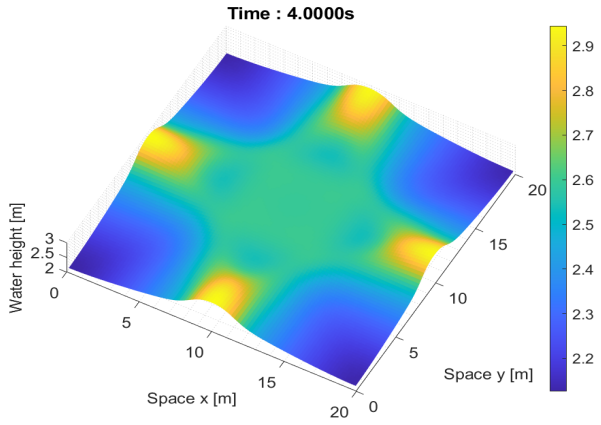

(f) $t = 4$s, first order scheme

Figure 7: Water drop in a basin; water height at time $t = 0$s, $t = 1$s, $t = 2$s, $t = 3$s and $t = 4$s. $M = 100$ cells, CFL$= 0.25$ and CFL$= 0.45$ for the 2D extension of second and first order scheme respectively.

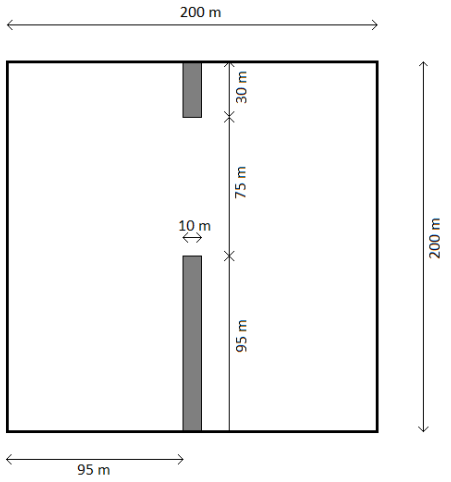

Figure 8: Geometry of the dam in the squared dam break test problem.

assume null velocities,

$$z(x,y,t=0) = \max(0, 0.25 - 5((x-0.5)^2 + (y-0.5)^2)) \quad \text{and} \quad h(x,y,t=0) = 0.5 - z(x,y).$$

Thus, the initial solution satisfies the "lake at rest" condition. Indeed, our 2D numerical schemes are able to preserve this kind of stationary solutions up to an error of order 10^{-15}.

5.9 Conical dune of sand

This test case has been vastly used to validate numerical schemes for shallow water Exner system, here we do refer for instance to [6, 33]. When considering the Grass formulation for the sediment discharge, we take porosity $\rho_0 = 0.4$, where we recall that $\zeta = \frac{1}{1-\rho_0}$. The domain is a $L \times L$ square with $L = 1000$m. At time $t = 0$, we impose

$$\begin{aligned}
z(x,y,t=0) &= \begin{cases} 0.1 + (\sin(\frac{\pi(x-300)}{200}))^2(\sin(\frac{\pi(y-400)}{200}))^2 & \text{if} \quad 300 \le x \le 500 \quad \text{and} \quad 400 \le y \le 600 \\ 0.1 & \text{otherwise,} \end{cases} \\
h(x,y,t=0) &= 10 - z(x,y,t=0), \\
u(x,y,t=0) &= \frac{10}{h(x,y,0)} \quad \text{and} \quad v(x,y,t=0) = 0.
\end{aligned}$$

Here, as boundary conditions, we assume that at the upstream we impose $u(x,y,t) = \frac{10}{h(x,y,t)}$ while the other boundaries are usual transmissive conditions.

Then, we consider two different cases: in the first one we take $A_g = 1$ and ending time $t_{\text{End}} = 500$s, thus we are assuming a fast interaction between the flow and the sediments. As second case, we diminish the value of A_g, namely we impose $A_g = 0.1$, thus the strength of the interaction decreases. The outputs for these two test cases can be found in pictures 10 and 11 respectively. The result are in agreement with the ones reported in [6] even if more diffusive due to a coarser mesh size ($M = 100$ cells).

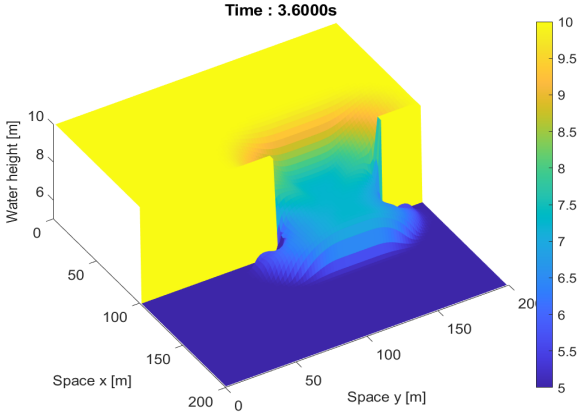

(a) $t = 3.6$s

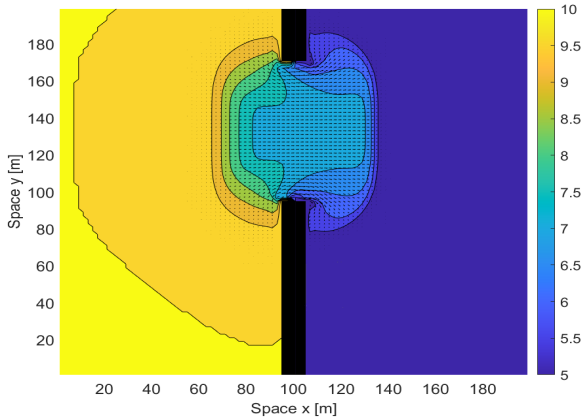

(b) $t = 3.6$s

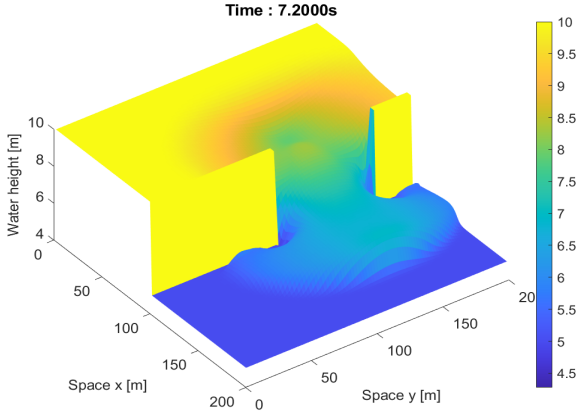

(c) $t = 7.2$s

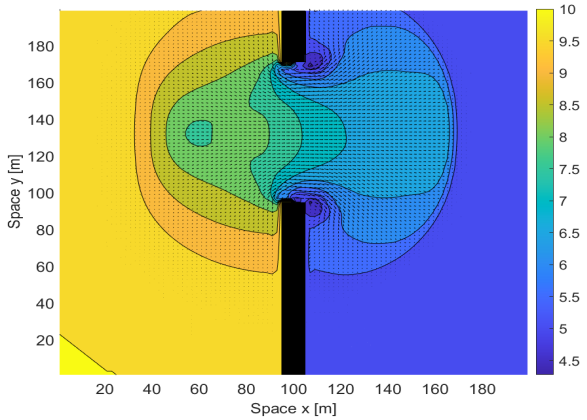

(d) $t = 7.2$s

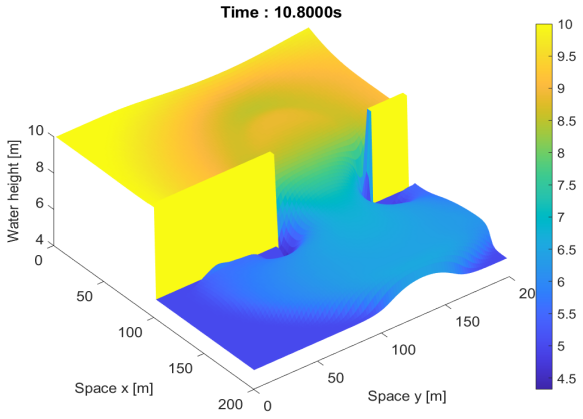

(e) $t = 10.8$s

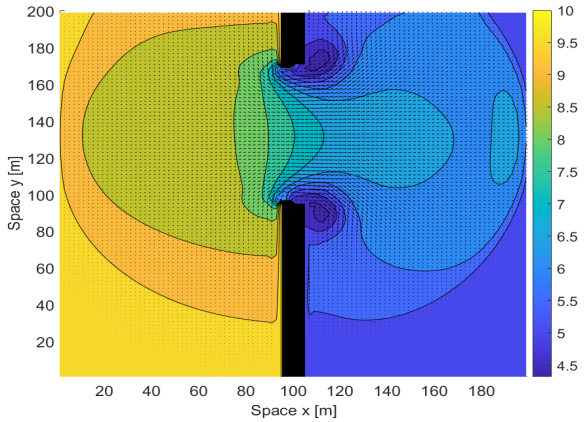

(f) $t = 10.8$s

Figure 9: Squared dam break; water height (left) and contour plot and velocity field (right) at time $t = 3.6$s, $t = 7.2$s and $t = 10.8$s. Dam in black. 2D extension of second order scheme with $M = 100$ cells and CFL$= 0.25$.

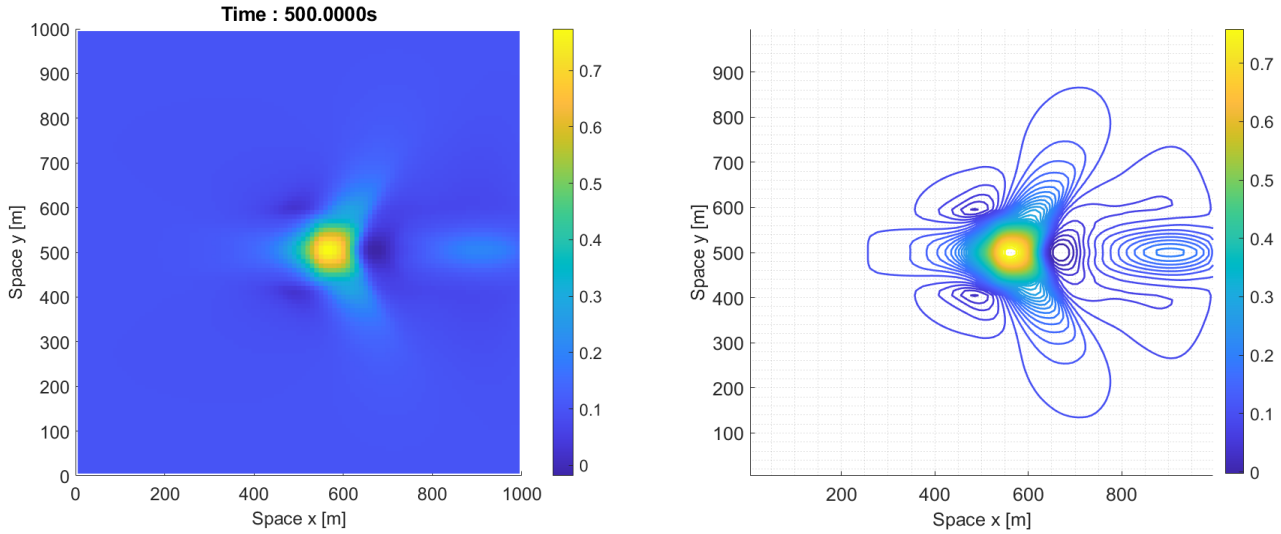

Figure 10: Conical dune of sand; fast interaction $A_g = 1$. Bed level (left) and contour plot (right) at time $t = 500$s. 2D extension of second order scheme with $M = 100$ cells and CFL$= 0.25$.

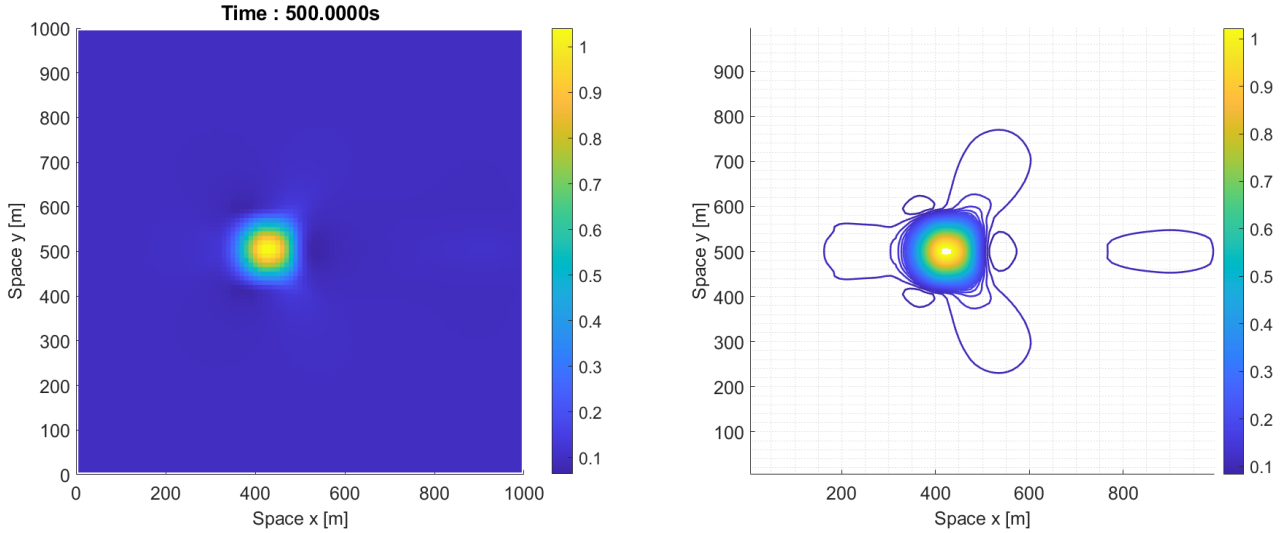

Figure 11: Conical dune of sand; fast interaction $A_g = 1$. Bed level (left) and contour plot (right) at time $t = 500$s. 2D extension of second order scheme with $M = 100$ cells and CFL$= 0.25$.

6 Concluding remarks

In this work a second-order well-balanced Lagrange-projection scheme for the shallow water Exner system has been presented in 1D. Two-dimensional extension is proposed as well. Numerical results proved the validity of the scheme. Generally, no oscillations are present in the numerical outputs, with the exception of one test case, in which it is shown that to slightly refine the mesh solve the mentioned problem. Further work to solve implicitly the acoustic step is required. Other strategies to take into account the Exner equation in the Lagrange-projection formalism are being explored and will be shortly submitted.

Acknowledgments

This work was partially supported by a grant from Région Île-de-France.

References

[1] A. Ambroso, C. Chalons, P.-A. Raviart. *A Godunov-type method for the seven-equation model of compressible two-phase flow.* Computers & Fluids. 54. 67-91. 10.1016/j.compfluid.2011.10.004. (2012).

[2] Emmanuel Audusse, Christophe Berthon, Christophe Chalons, Olivier Delestre, Nicole Goutal, Magali Jodeau, Jacques Sainte-Marie, Jan Giesselmann, Georges Sadaka. *Sediment transport modelling : Relaxation schemes for Saint-Venant – Exner and three layer models.* ESAIM: Proc. 38 78-98 (2012). DOI: 10.1051/proc/201238005

[3] E. Audusse, F. Bouchut, M.O. Bristeau, R. Klein and B. Perthame. *A fast and stable well-balanced scheme with hydrostatic reconstruction for shallow water flows.* SIAM Journal on Scientific Computing, 25:2050–2065, 2004.

[4] Emmanuel Audusse, Marie-Odile Bristeau. *A 2d Well-balanced Positivity Preserving Second Order Scheme for Shallow Water Flows on Unstructured Meshes.* [Research Report] RR-5260, INRIA. 2004, pp.31.

[5] E. Audusse, C. Chalons, P. Ung. *A simple three-wave approximate Riemann solver for the Saint-Venant-Exner equations.* Int J Numer Meth Fluids. 2018; 87:508–528.

[6] Emmanuel Audusse, Olivier Delestre, Le Minh-Hoang, Mathias Masson-Fauchier, Pierre Navaro, et al.. *Parallelization of a relaxation scheme modelling the bedload transport of sediments in shallow water flow.* ESAIM: Proceedings, EDP Sciences, 2013, 43, pp.80-94. ff10.1051/proc/201343005ff. ffhal00840200

[7] Christophe Berthon, Stéphane Cordier, Minh Le, Olivier Delestre. *An analytical solution of Shallow Water system coupled to Exner equation.* Comptes Rendus Mathématique, Elsevier Masson, 2012, 350 (3-4), pp.183-186.

[8] François Bouchut, Christophe Chalons, Sébastien Guisset. *An entropy satisfying two-speed relaxation system for the barotropic Euler equations. Application to the numerical approximation of low Mach number flows.* Numerische Mathematik, Springer Verlag, 2020, 145, pp.35-76. ff10.1007/s00211-020- 01111-5ff. ffhal-01661275v2f

[9] R. Briganti, N. Dodd, D. Kelly, and D. Pokrajac. (2012). *An efficient and flexible solver for the simulation of the morphodynamics of fast evolving flows on coarse sediment beaches.* International Journal for Numerical Methods in Fluids. 69. 859 - 877. 10.1002/fld.2618.

[10] M. J. Castro Díaz, E. D. Fernández-Nieto and A.M. Ferreiro. *Sediment transport models in Shallow Water equations and numerical approach by high order finite volume methods.* Computers & Fluids, Volume 37, Issue 3, 2008, Pages 299-316.

[11] M. J. Castro Díaz, E. D. Fernández-Nieto, A.M. Ferreiro and C. Parés. *Two-dimensional sediment transport models in shallow water equations. A second order finite volume approach on unstructured meshes.* Computer Methods in Applied Mechanics and Engineering. 198. (2009). 2520-2538. 10.1016/j.cma.2009.03.001.

[12] Christophe Berthon, Françoise Foucher. *Efficient well–balanced hydrostatic upwind schemes for shallow–water equations.* 2012. Journal of Computational Physics. 231. 4993–5015. 10.1016/j.jcp.2012.02.031.

[13] Marie Billaud Friess, Benjamin Boutin, Filipa Caetano, Gloria Faccanoni, Samuel Kokh, et al.. *A second order anti-diffusive Lagrange-remap scheme for two-component flows.* ESAIM: Proceedings, EDP Sciences, 2011, 32, pp.149-162. ff10.1051/proc/2011018ff. ffhal-00708605f

[14] François Bouchut. *Nonlinear stability of finite volume methods for hyperbolic conservation laws and well-balanced schemes for sources.* Frontiers in mathematics, 2004.

[15] Manuel J. Castro Díaz, Christophe Chalons and Tomás Morales De Luna. *A fully well-balanced Lagrange-Projection type scheme for the Shallow-water equations.* 2018. SIAM J. Numer. Anal., 56(5), 3071–3098.

[16] Manuel J. Castro Díaz, Enrique D. Fernández-Nieto, Tomás Morales de Luna, Gladys Narbona-Reina and Carlos Parés. *A HLLC scheme for nonconservative hyperbolic problems. Application to turbidity currents with sediment transport.* 2013. European Series in Applied and Industrial Mathematics (ESAIM): Mathematical Modelling and Numerical Analysis. 47. 10.1051/m2an/2012017.

[17] M.J. Castro, T. Morales de Luna and C. Parés. *Well-Balanced Schemes and Path-Conservative Numerical Methods.* Handbook of Numerical Analysis, Vol. 18. 2017. Pages 131-175.

[18] Manuel J. Castro Díaz, Alberto Pardo Milanés and Carlos Parés. *Well-balanced numerical schemes based on a generalized hydrostatic reconstruction technique.* Mathematical Models and Methods in Applied SciencesVol. 17, No. 12, pp. 2055-2113 (2007)

[19] Manuel J. Castro and Carlos Parés. *Well-Balanced High-Order Finite Volume Methods for Systems of Balance Laws.* Journal of Scientific Computing volume 82, Article number: 48 (2020)

[20] Christophe Chalons, Mathieu Girardin, Samuel Kokh. *An all-regime Lagrange-Projection like scheme for 2D homogeneous models for two-phase flows on unstructured meshes.* Journal of Computational Physics, Elsevier, 2017, 335, pp.885-904. 10.1016.

[21] Christophe Chalons, Mathieu Girardin, Samuel Kokh. (2014). *An All-Regime Lagrange-Projection Like Scheme for the Gas Dynamics Equations on Unstructured Meshes.* Communications in Computational Physics. 20. 10.4208/cicp.260614.061115a.

[22] Christophe Chalons, Pierre Kestener, Samuel Kokh, and Maxime Stauffert. *A large time-step and well-balanced Lagrange-Projection type scheme for the Shallow-water equations.* 2016. Communications in Mathematical Sciences. 15. 10.4310/CMS.2017.v15.n3.a9.

[23] Christophe Chalons, Samuel Kokh, Mathieu Girardin. (2013). *Large Time Step and Asymptotic Preserving Numerical Schemes for the Gas Dynamics Equations with Source Terms.* SIAM Journal on Scientific Computing. 35. 10.1137/130908671.

[24] F. Coquel, E. Godlewski, B. Perthame, A. In, and P. Rascle.*Some new Godunov and relaxation methods for two-phase flow problems.* Godunov methods (Oxford, 1999), pages 179–188, 2001.

[25] F. Coquel and B. Perthame. *Relaxation of energy and approximate Riemann solvers for general pressure laws in fluid dynamics.* SIAM Journal on Numerical Analysis, 35(6):2223–2249, 1998.

[26] Stéphane Cordier, Minh Le, Tomas Morales de Luna. *Bedload transport in shallow water models: why splitting (may) fail, how hyperbolicity (can) help.* Advances in Water Resources, 34(8): 980–989. August 2011.

[27] Frédéric Duboc, Cédric Enaux, Stéphane Jaouen, Hervé Jourdren, Marc Wolff. *High-order dimensionally split Lagrange-remap schemes for compressible hydrodynamics.* Comptes Rendus Mathematique Volume 348, Issues 1–2, January 2010, Pages 105-110.

[28] G. Gallice. *Solveurs simples positifs et entropiques pour les systèmes hyperboliques avec terme source.* C. R. Math. Acad. Sci. Paris 334, no. 8, pp. 713-716, (2002).

[29] G. Gallice. *Positive and entropy stable Godunov-type schemes for gas dynamics and MHD equations in Lagrangian or Eulerian coordinates.* Numer. Math. 94 no. 4, pp. 673-713, (2003).

[30] J. C. González-Aguirre, M.J. Castro, T. Morales de Luna. *A robust model for rapidly varying flows over movable bottom with suspended and bedload transport: modelling and numerical approach. Advances in Water Resources* Volume 140, June 2020, 103575.

[31] Sigal Gottlieb and Chi-Wang Shu. *Total variation diminishing RUNGE-KUTTA schemes.* 1996. Mathematics of Computation. 67. 10.1090/S0025-5718-98-00913-2.

[32] A. Harten, P.D. Lax, and B. Van Leer. *On upstream differencing and Godunov-type schemes for hyperbolic conservation laws.* SIAM Review, 25:pp. 35–61, 1983.

[33] J. Hudson. *Numerical techniques for morphodynamic modelling.* PhD thesis, University of Reading, October 2001.

[34] C. Juez, J. Murillo, P. García-Navarro. *A 2D weakly-coupled and efficient numerical model for transient shallow flow and movable bed.* Advances in Water Resources Volume 71, September 2014, Pages 93-109.

[35] Raphaël LOUBERE. *Une Méthode Particulaire Lagrangienne de type Galerkin Discontinu Application à la Mécanique des Fluides et l'Interaction Laser/Plasma.* These doctorale. 2002.

[36] Xin Liu, Abdolmajid Mohammadian, Alexander Kurganov, Julio Angel Infante Sedano. *Well-balanced central-upwind scheme for a fully coupled shallow water system modeling flows over erodible bed.* Journal of Computational Physics, Volume 300, 1 November 2015, Pages 202-218.

[37] Pierre-Henri Maire, Rémi Abgrall, Jérôme Breil, Jean Ovadia. *A Cell-Centered Lagrangian Scheme for Two-Dimensional Compressible Flow Problems.* 2007. SIAM Journal on Scientific Computing. 10.1137/050633019.

[38] Victor Michel-Dansac, Christophe Berthon, Stéphane Clain, Françoise Foucher. *A well-balanced scheme for the shallow-water equations with topography.* Computers and Mathematics with Applications. 72. 10.1016/j.camwa.2016.05.015. (2015)

[39] Victor Michel-Dansac, Christophe Berthon, Stéphane Clain, Françoise Foucher. *A well-balanced scheme for the shallow-water equations with topography or Manning friction.* Journal of Computational Physics, Elsevier, 2017, 335, pp.115-154.

[40] Tomás Morales De Luna, Manuel J. Castro Díaz and Christophe Chalons. *High order fully well-balanced Lagrange-Projection scheme for Shallow-water.* Commun. Math. Sci., Vol. 18, No. 3, pp. 781–807 (2020)

[41] Tomás Morales de Luna, Manuel J. Castro Díaz, Carlos Parés Madroñal, Enrique D. Fernández-Nieto. *On a Shallow Water Model for the Simulation of Turbidity Currents.* (2009). Communications in Computational Physics - COMMUN COMPUT PHYS. 6. 10.4208/cicp.2009.v6.p848.

[42] J. Murillo and P. García-Navarro. *An Exner-based coupled model for two-dimensional transient flow over erodible bed.* Journal of Computational Physics, Volume 229, Issue 23, p. 8704-8732. Nov 2010.

[43] Raimund Bürger, Christophe Chalons and Luis Villada. *Antidiffusive and Random-Sampling Lagrangian-Remap Schemes for the Multiclass Lighthill-Whitham-Richards Traffic Model.* SIAM Journal on Scientific Computing. 35. 10.1137/130923877. (2013).

[44] Mohammed Seaïd. *Non-oscillatory relaxation methods for the shallow-water equations in one and two space dimensions.* (2004). International Journal for Numerical Methods in Fluids. 46. 457 - 484. 10.1002/fld.766.

[45] E. F. Toro and A. Siviglia. *PRICE: Primitive Centred Schemes for Hyperbolic Systems.* 2003. International Journal for Numerical Methods in Fluids. 42. 1263 - 1291. 10.1002/fld.491.

[46] E. F. Toro. *Riemann Solvers and Numerical Methods for Fluid Dynamics*, Third Edition. Springer– Verlag, 2009.

[47] C. B. Vreugdenhil. *Numerical Methods for Shallow Water Flow.* Dordrecht ; Boston: Kluwer Academic Publishers (1994). Part of the Water Science and Technology Library book series (WSTL, volume 13).